Structures 31 (2021) 462–483

Contents lists available at ScienceDirect

Structures

journal homepage: www.elsevier.com/locate/structures

A new methodology using beam elements for the analysis of steel frames subjected to non-uniform temperatures due to fires

Myriam R. Pallares-Muñoz [a,b,*], Ignacio Paya-Zaforteza [a], Antonio Hospitaler [a]

[a] Universitat Politècnica de València, ICITECH, Camino de Vera S/N, 46022 València, Spain
[b] Universidad Surcolombiana, Cra 1 Aven. 26, 410003 Neiva, Colombia

ARTICLE INFO

Keywords:
New methodology
Low-cost computational methodology
Thermo-mechanical phenomenon
Fire situation
Non-uniform temperatures
Cardington test

ABSTRACT

Non-uniform heating in structures under fire involves the appearance of 3D-phenomena and typically requires the use of complex models built with finite elements shell or solid. Although different procedures have been developed to model the complex thermo-mechanical phenomenon, there is no simple, accurate, and low-cost computational methodology involving the space–time variation of the temperature and displacement fields that opens the path advancing more easily towards modeling more complex structural problems in a fire situation. To overcome this knowledge-gap, this paper presents a new methodology that fulfills those conditions, making it possible to carry out more complex analyses that require many simulations in a short time and at low computational costs. The new methodology to obtain the thermo-mechanical response to non-uniform heating and mechanical loads is general, simple, accurate, and avoids using complex and high-cost finite elements, simplifying the structural modeling, and reducing the computational analysis cost. As a result, complex structural fire engineering problems such as probabilistic and optimization analysis can be handled much more easily, representing a significant step toward the generalized application of performance-based approaches to deal with fire effects on structures. The procedure uses simple but advanced Timoshenko's beam-type finite elements and represents the non-uniform temperature space–time field through a mean value of the temperature and the two mean values of the section thermal gradients which are variable in time during the fire. The methodology is satisfactorily validated with results (experimental and numerical) of the Cardington frame test and captures 3D-phenomena such as buckling, flexural–torsional buckling, and warping.

1. Introduction

Steel frames define the skeleton of many residential, commercial, industrial, and office buildings. In fact, according to data from the Council on Tall Buildings and Urban Habitat, in early 2020, 67% of the world's 100 tallest buildings used steel or steel–concrete composite structural systems [1]. Fire is one of the main hazards that can affect steel and composite constructions and was responsible, e.g., for the collapse of the World Trade Center Twin Towers after they were hit by airplanes [2–4].

This vulnerability of steel and composite buildings vis-à-vis fire hazards has motivated the development of methodologies to predict structures response to fire. These methodologies typically have three components: a fire model that represents the effects of fire in the environment of the structure, a thermal model that predicts the temperatures in the structural members, and a mechanical model that gives the response of the structure caused by mechanical and thermal stresses. For the fire model, there are two design strategies. The most common fire design strategy is the prescriptive approach where a nominal fire curve represents the fire (e.g., the ISO 834 fire curve), and the structure is requested to resist the effects of this fire curve for a code-specified time. More advanced is the use of a performance-based approach, where an effort is made to represent the physical fire features. To do so, fire models of different complexity are available (e.g., parametric fires, localized fires, zone models, or computational fluid dynamics -CFD-models). More realistic models, such as localized fires or CFD [5–8], do not uniformly heat the structure and, therefore, impose non-uniform temperature and heat flux fields that should be properly included in the models. Besides, when a performance-based approach is used, the analysis can include a single member, a part of the structure [9], or the

* Corresponding author at: Universitat Politècnica de València, ICITECH, Camino de Vera S/N, 46022 València, Spain.
E-mail addresses: myriam.pallares@usco.edu.co, mypalmuo@doctor.upv.es (M.R. Pallares-Muñoz), igpaza@cst.upv.es (I. Paya-Zaforteza), ahospitaler@cst.upv.es (A. Hospitaler).

https://doi.org/10.1016/j.istruc.2021.02.008
Received 17 November 2020; Received in revised form 6 January 2021; Accepted 3 February 2021

entire structure, the latter two cases requiring the use of advanced calculation models [10]. These models can be built using the beam, shell [11], or solid finite elements [12], being beam elements especially appealing because of their much easier modeling and lower computational cost, which results in savings in modeling times, CPU-times, memory, and storage demands. However, the use of beam elements to model the response of structures to realistic fires is very challenging due to, among other reasons, the problems to adequately reproduce phenomena such as web buckling and the difficulty to properly discretize the temperature in the cross-section of the elements when longitudinal and/or transversal thermal gradients are present. These gradients appear, e.g., when the temperature fields around the structure are not uniform as it is the case for bridges [10,13,14] and perimeter columns [15], and/or when the steel members are joined to or protected by concrete elements [16].

Achieving a good approximation of the non-uniform temperature in the beam section is justified insofar as the accurate calculation of material properties, non-linear stress–strain relationships, and thermal strains depend on a good approximation of the temperature in the beam section. Therefore, the structure's response is more realistic, as long as the temperature field in the beam cross-section is as well modeled as possible. A common approach to represent non-uniform temperature fields, i.e., thermal gradients, within the cross-section of a structural element is the use of multiplier values applied to the parts of the cross-section (e.g., the web and the two flanges). These multipliers are calculated as temperature factors from a pattern-curve, which, in some cases, is the gas compartment temperature [17] and, in others, it is the curve of the temperatures of one of the section parts [18]. As a result, the patterns of the temperature evolution are the same in the entire section. Additionally, it is also common to assume a uniform temperature by parts (i.e., web and two flanges), or, e.g., a linear temperature variation with distance from the top/bottom face of the cross-section (linear interpolation along the vertical axis of the cross-section).

Several authors have taken all or part of these approaches to use beam elements from several software packages such as Ansys, Abaqus, LS-Dyna, Vulcan, and Safir to model structures under fire. Burges and Alexandrou used Vulcan software to apply different factorized temperatures to each part of an I-profile section steel beam in fire based on the gas temperature curve [19–21]. Santiago *et al.* built a structural 2D-model of the Cardington framework fire test using Abaqus and Safir beam elements and applied a linear temperature variation constant through time within the vertical direction of the section steel members [18,22]. To do so, they first calculated the temperature time-history at a representative part of the cross-section with a 2D-heat transfer analysis, which then is scaled to obtain the time-history at other representative parts. Kumar *et al.* applied a linear temperature variation in the vertical direction of the I-profile section steel members of a framework tested in fire using Ansys beam elements [23]. To do so, they first built a thermal model of the entire framework using shell elements to know the temperatures at specific framework cross-sections; then, they determined the average temperature in those sections and in the two flanges to calculate between these three values a linear vertical variation of the temperature of each section that they later applied to the beam elements of a structural model. Therefore, section temperature distributions based on multipliers and pattern-curves have been used but have several disadvantages because they depend on a very good definition of the multipliers that remain constant throughout the fire and only consider the temperature variations in the web direction. They cannot represent the changes produced in the heating/cooling speed of the section points in the presence of isolation elements. In addition, these approaches that have involved section heat transfer analysis have only used temperature results and have ignored the importance of thermal gradients responsible for temperature changes in both directions of the section. Moreover, the disadvantage of entire member heat transfer analyses using shell or solid elements is they are very robust and involve unnecessary modeling effort compared to the information that can be processed from them when structural models are built with beam elements. On the other hand, the heat transfer analyses only of the sections with plane elements allow a good detail of the section thermal phenomenon characteristics. They are also easier to model and collect adequate and enough information on the thermal phenomenon of each section.

More advanced is the LS-Dyna software beam element approach, based on the formulation of a degenerated solid element where the temperatures at the integration points are interpolated from the temperature–time and natural coordinates of points temperature are applied. Rackauskaite *et al.* used LS-Dyna to build a 2D-model of the Cardington framework. These authors directly applied the temperature–time curves at the three points where the experiment temperature was measured [24]. The LS-Dyna beam element has two drawbacks. First of all, it uses a very specific formulation that cannot be used in other software. Secondly, LS-Dyna is an explicit analysis software, i.e., it uses explicit dynamics algorithms in which very small-time steps are required to maintain the calculations numerical stability. By contrast, fire phenomena in structures before collapsing do not take place in microseconds or seconds (as it happens, e.g., in impacts, explosions, collisions, and even earthquakes) but last minutes and, in some cases, even hours. Therefore, fire modeling in structures with explicit techniques requires many time steps that must be calculated one by one sequentially in time, i.e., the parallelism of computing can only be used for the subdivision of spatial domains.

Within this context, this paper proposes a simple new general systematic methodology to model steel structures behavior under fire in non-uniform temperature conditions (i.e., under longitudinal and/or transversal thermal gradients). This methodology uses beam elements that incorporate the two spatially and temporally variable thermal gradients of the section from the thermal model and, therefore, reproduce the time-dependent thermal and mechanical structural response. Triangle-shape plane elements with quadratic approximation in the 2D-thermal model and seven-degree Timoshenko's beam elements in the 2D/3D mechanical models are used. This methodology is validated with the full-scale experimental measurements carried out in Cardington published in [25,26], and the 2D-numerical simulations carried out by Franssen *et al.* and Santiago *et al.* [18,22,27]. The document is structured as follows: Section 2 describes the Cardington test used to validate the proposed methodology; Section 3 presents details of both the proposed methodology and the model of the Cardington framework used for validation purposes; Section 4 presents an in-depth analysis of the temperature and thermal gradient results of the heat transfer models of the Cardington framework; Section 5 presents the results of the mechanical framework models which are validated with the measured displacements, and the 2D-numerical simulations of the framework carried out by Santiago *et al.* [18,22]. Section 5 also presents a detailed analysis of the results of a Cardington framework 3D-mechanical model, including flexural-torsion effects, 3D-displacement fields, and plastic deformations. Finally, in Section 6, the main conclusions of the research are drawn.

2. Cardington fire test

The experiment to validate the methodology to approximate the effects of non-uniform heating in the section and evaluating the influence of thermal expansion, lateral restraint, and the effects of 3D-modeling, was conducted by Latham *et al.* [25] on a loaded steel 2D-framework located inside a compartment built in Cardington for fire testing (Fig. 1). The beam of the framework is a 4.550 m length UB 406x178x54 profile. This profile was bolted to two columns materialized with a UC 203x203x52-profile of 3.530 m in height. The columns were filled with autoclaved aerated concrete blocks between the flanges to protect the web from fire, and a concrete slab was used on the beam to provide thermal insulation. A specially designed subsidiary framework avoided lateral and swaying instabilities. Loads were applied to columns and at four points along the beam through hydraulic jacks and remained

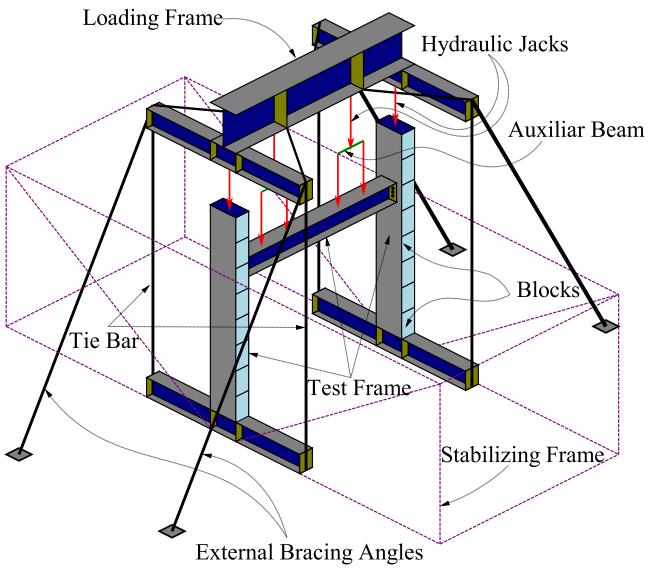

Fig. 1. Cardington framework.

constant in the fire test. The test lasted 30 min, and maximum temperatures above 750 °C on the beam and above 606 °C were observed on the column.

3. Numerical modeling

Due to the symmetry, the only half framework was modeled, and one spring was placed at the height of 3210.1 mm to represent the secondary framework support. Cardington framework was modeled in 2D and 3D; however, because the beam-finite element used for the modeling is 3D, out-of-plane translation constraints were added to the framework nodes to simplify that dimension in the 2D-model. Concrete elements in the framework only fill an insulating role, so they only participate in the thermal resistance but not in the structural response.

2D simulations of the Cardington experiment have been carried out by Franssen *et al.* and Santiago *et al.* using the Ceficoss, Safir, and Abaqus software [18,22,27]. However, the work presented in this paper introduces the following contributions:

- The development of a simple methodology with beam elements to determine adequately and rigorously, the response to fire of steel frames subjected to non-uniform temperatures, spending less modeling effort, and calculation time against more complex models built with finite elements of a higher level of discretization such as shells or solids.
- The use of Ansys for modeling heat transfer in the steel framework member sections and the loaded framework nonlinear mechanical modeling.
- The use of the complete thermal response of the analyzed cross-sections to formulate the new methodology representing the non-uniform temperature field in the sections (variable in space and time), based on the average values of the temperature and the elementary thermal gradients.
- The detailed description through flowcharts of the procedures for: i) the calculation of average temperature and thermal gradients, which approximate the non-uniform temperature field within the structural elements, ii) applying these components in the discrete 3D- finite element beam sections, and iii) the nonlinear mechanical analysis of the loaded framework.
- The representation of calculated temperature surfaces in the sections and applied temperature approximation planes.
- The time-history results of temperature distribution and thermal gradients in the sections of the analyzed framework sections.
- The bi-laminate effect analysis caused by the section internal thermal gradients when the members are not heated uniformly around the perimeter.
- The calculation of the temperature variation factors throughout the beam.
- The inclusion of a Timoshenko's 3D-beam element with the ability to: i) including cross-section warping, ii) adequately reproduce the 3D-field of displacements when the element is subjected to non-uniform temperatures, iii) the deformability of the cross-section (Poisson effect), and iv) correctly model the mechanical 3D-response of the steel framework.
- The inclusion of thermal deformations and self-weight loads in the mechanical analysis to consider additional bending deformations into the framework response.
- Column's mid-height deflection and top-end extension calculation at the pseudo-mesh nodes of the beam finite element section, and displaying these results at the nodes of the beam element outer face (in extruded view).
- The following calculations on the members of the 3D framework (extruded view): i) the displacement of the column perpendicular to the plane of the framework, ii) the applied 3D temperature field, iii) the plastic deformation components produced by mechanical and thermal loads, iv) the flexural–torsional buckling of the column and, v) the warping, the bimoment, and the bicurvature.
- The reduction of the time required to model and calculate 2D and 3D structures under fire.

4. Methodology description

In this research, the Cardington steel framework was modeled in Ansys using 3D-beam structural elements. These finite elements only have displacement-degrees of freedom and do not allow discretizing the temperature in the cross-section. Consequently, the non-uniform and time-varying temperature cannot be directly introduced into the beam structural finite element cross-section. However, it allows specifying an elemental uniform temperature and temperature gradients that vary linearly both in the cross-section and in the element length. For that reason, a methodology that approximates the non-uniform temperature distribution in the section of a 3D-beam structural finite element (Fig. 2 (a)) through the following three time-varying components has been proposed:

a) A uniform temperature component equal to the average section temperature, variable in time (Fig. 2(b)).
b) A temperature gradient component that varies linearly about the Y-axis: this component is equal to the section average horizontal gradient, variable in time (Fig. 2(c)).
c) A temperature gradient component that varies linearly about the Z-axis: this component is equal to the section average vertical gradient, variable in time (Fig. 2(d)).

The Y and Z-axes used to describe the direction of the gradients match the 3D-beam structural finite element local directions (see Fig. 10 (a)).

In Fig. 2(a), the time-varying non-uniform temperature in the 3D-beam finite element section is represented by three time-varying average components (Fig. 2(a-c)). Thus, the temperature applied at a point of the 3D-beam finite element section (for each time) can be determined through the three time-varying components of the non-uniform temperature described. Since 3D-beam-type finite elements are used, the average temperature component is applied at the centroid so that the temperature applied at one point of the 3D-beam section can be approximated by Eq. (1).

$$T(Y,Z,t) \approx T_{avg.}(t) + TGy_{avg}(t) \times Y + TGz_{avg}(t) \times Z \quad (1)$$

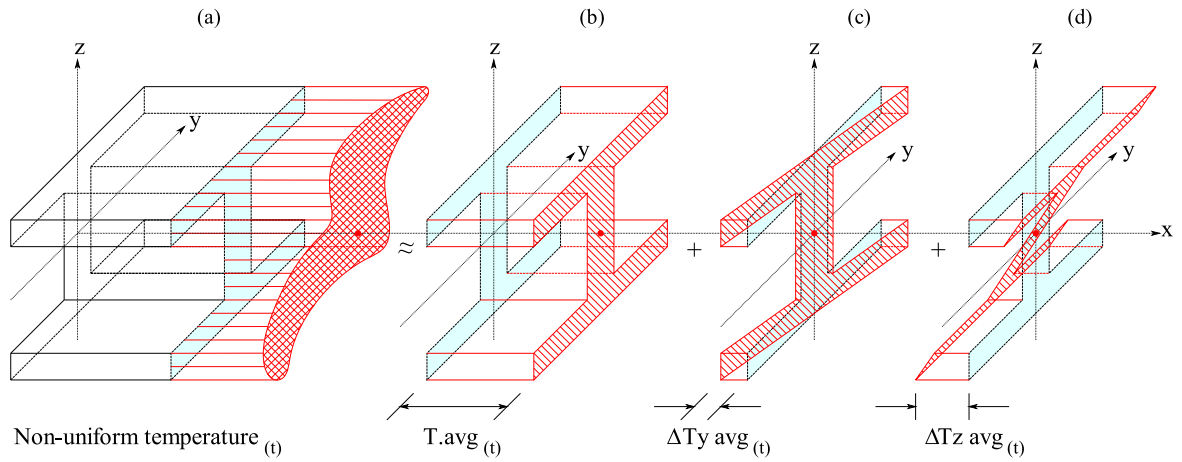

Fig. 2. Representation of the temperature profile components referred to a 3D-beam finite element local axes.

In Eq. (1), T_{avg} is the average section temperature applied at the centroid, TGy and TGz are the positive or negative average horizontal and vertical gradient values of the section, respectively, and Y, Z are the coordinates (positive or negative) of the point, according to its position concerning the origin of the reference system located at the centroid of the section. In Eq. (1), lines of average gradients pass through the section centroid so that average gradient components are null at the centroid, and the temperature applied at the centroid is equal to the average section temperature.

Non-uniform temperature components in Fig. 2(a-c) are determined by carrying out thermal analyses of the framework sections. Thus, the full methodology requires that the following procedures to be performed:

1) 2D-thermal analysis of each framework mixed-section with plane elements is done to obtain the thermal response, i.e., the time-histories of temperature and thermal gradients (horizontal and vertical) in all of the mesh's finite elements.
2) The steel section results are separated to determine only the thermal response in this material because concrete elements are not present in the structural model.
3) Average temperature (Avg_Temp) and average thermal gradients (Avg_Grad_YY and Avg_Grad_ZZ) of the steel-section are calculated at each time to obtain the time-history results of each one. For calculating these three time-varying average components (see Fig. 2), the thermal gradient results in the steel section's finite elements are averaged in each direction at each time. Temperature results are also averaged in the steel section's finite elements to obtain a temperature mean value of the steel-section at each time.
4) The framework's structural model is built with 3D-beam finite elements, where the time-varying non-uniform temperature applied in the 3D-beam finite element section is represented by the three time-varying average components calculated from the section heat transfer models previously done. In this approach, average temperature and average gradients in the section vary at each time during the whole fire scenario.
5) Static geometrically and materially nonlinear analysis (GMNA) of the framework is done to determines the framework's fire resistance time and the structural response to this failure time.

In this new proposal, the variation of the two average gradient components of the section in time makes the temperature applied to the 3D-beam element section be variable in the two directions of the section at each time; i.e., a non-uniform temperature is defined in both directions of the section at each time of the fire scenario. This temperature field varying spatially and temporally affects the temperature-dependent material properties. The elastic modulus, the steel stress–strain behavior, and the thermal expansion also change as a function of the steel temperature in space and time [28].

This simple methodology makes reasonable and natural use of gradient results of the section's thermal model to represent as closely as possible the non-uniform time-varying temperature field that is applied in the 3D-beam steel section when this type of finite element is used to model the response of a structure in a fire situation. It is essential to highlight that the present methodology, unlike others [17–23], uses all available results of the heat transfer analysis in the section, i.e., all of the elemental temperature and elemental thermal gradients results.

A summary of the methodology is presented in Fig. 3.

Details of the full methodology are shown in Figs. 7, 8, and 13.

The methodology also includes the time-varying temperature in the framework beam's length, as Franssen recommended [27]. This longitudinal variation of the temperature in the framework's beam is approximated through reduction factors (fx) determined by a sinusoidal function, which varies between 0.90 approx. (at the beam/column connection, according to EN 1993-1-2 [29]) and 1.00 (at mid-span), considering that the fire location is at the beam mid-span. Thus, the reduction factors (fx) are calculated at the mid-point of each 3D-beam finite element that discretizes the framework's beam. Then, the factor (fx) at the midpoint of each 3D-beam finite element is multiplied by the average temperature component of the section (T_{avg} in Fig. 2(b)) to include a variation of the temperature in length. Since the average temperature component applied to the 3D-beam finite element section varies in time, the temperature along the beam also varies in time.

5. Heat transfer analysis of the framework sections

A complete heat transfer analysis was carried out with Ansys to determine the heat transferred to the framework sections. The thermal model includes conduction and convective-radioactive boundary conditions. The Cardington framework steel–concrete mixed-sections (beam-slab and column-block) for the transient thermal modeling are detailed in Fig. 4.

The specific heat (C_a), and thermal conductivity (λ_a) of steel with temperature were determined according to EN 1993-1-2 [29]. The convective heat transfer coefficient (α_c = 25 W/m^{2}K), the resulting emissivity between the fire source and the steel (ε_{res} = 0.7), and the radioactive shading effect on the outer flange of the column (ε = 0.3) were taken from [22]. The density (ρ_a) of steel was assumed to be independent of temperature with a constant value of 7850 kg/m^3. Variations of the specific heat (C_p) and thermal conductivity (λ_c) with the temperature of the concrete slab were determined according to EN 1992-1-2 [30]. The convective heat transfer coefficient (α_c) and the

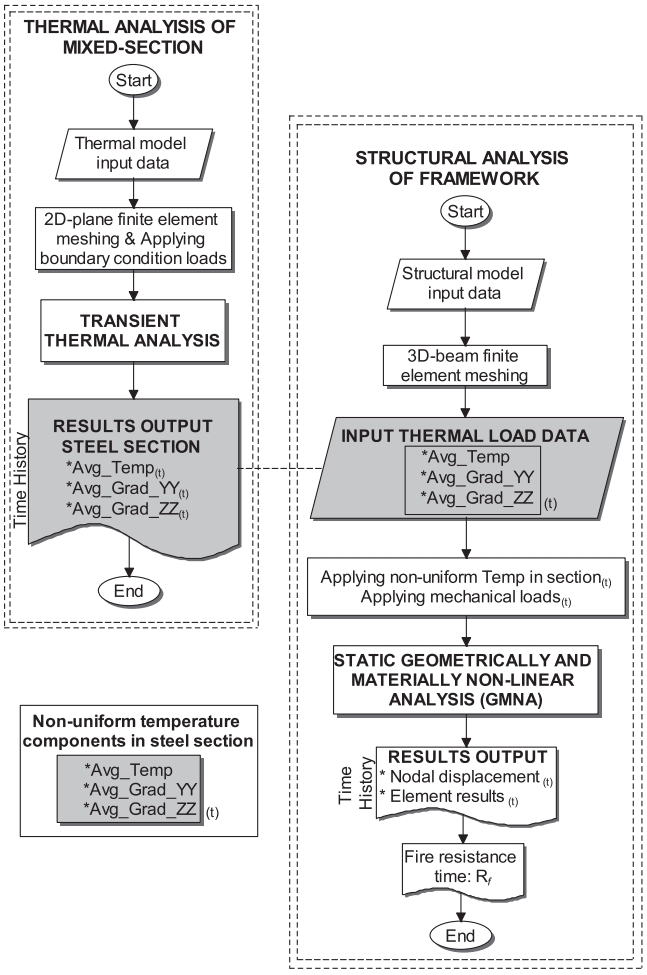

Fig. 3. Methodology summary.

resulting emissivity between the fire source and the concrete slab (ε_{res}) were 25 W/m^{2}K and 0.8, respectively. The density (ρ_c) of the concrete slab was assumed to be independent of temperature with a constant value of 2400 kg/m^3. For the concrete blocks isolating the column, a variation of thermal conductivity (λ_c) given by $0.20 + 0.0004\theta_a$ was considered, and the specific heat and density properties were assumed to be constant values of 1050 J/kg-K and 677 kg/m^3, respectively. Franssen *et al.* and Santiago *et al.* used these thermal properties of the concrete blocks in the Cardington framework thermal simulations [18,22,27].

The discretization is carried out for: i) the UB 406x178x54 steel beam section, attached to the 1200x150 mm concrete slab section and, ii) the UC 203x203x52 steel column section attached to the aerated concrete block sections on the flanges to provide thermal insulation. Direct contact between the steel section and the concrete was assumed (as in the Cardington test) in order to consider the heat transferred from the steel section to the concrete. Concrete elements produce non-uniform temperature distributions in the beam and column steel-sections.

The temperature of the environment (combustion gases) is the main parameter that affects the heat exchange between the environment (the fire) and the structure. The temperature of these environment combustion gases in the experiment was measured for 30 min. The evolution of the gas temperature over time (natural fire curve) is shown in Fig. 5 [22].

Based on the thermal properties and the convection-radiation boundary conditions, 2D-heat transfer models of the steel beam-concrete slab and steel column-concrete blocks sections have been done in Ansys using PLANE35 elements. This finite element is a quadratic triangle of six (6) nodes, with a degree of freedom (temperature) per node, applicable to the transient state 2D-thermal analysis. Convection and radiation are introduced as surface loads at the model boundaries of each section.

The heat transfer analysis allows knowing the variation in space and time of the temperature field and the thermal gradient field in the section. This variation in temperature and gradients is the starting point for the methodology presented in this paper.

Fig. 6 shows the discretization of the beam-slab and column-block sections with PLANE35 elements. These meshes do not require great refinements since the finite element shape functions introduce a quadratic approximation of the temperature. Unstructured meshes of

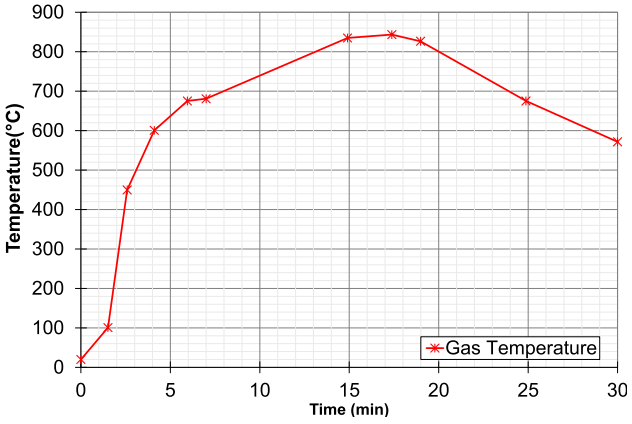

Fig. 5. Natural fire curve.

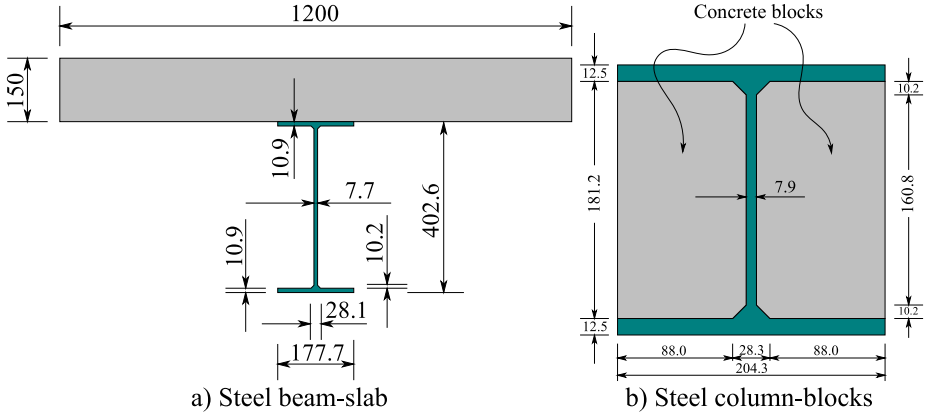

Fig. 4. Mixed cross-sections dimensions.

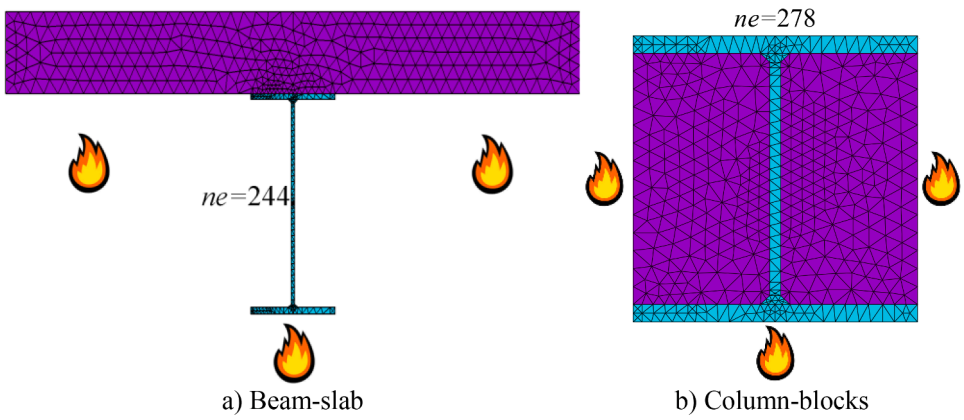

Fig. 6. Cross-sections discretization.

triangular-shaped elements are used because of the adaptability to the section shape (fillet zones) and the good aspect ratio, so that very good meshes are automatically generated. The number of elements *ne* in the beam and column steel sections is shown in Fig. 6(a,b).

The beam and column steel-section temperatures obtained from the thermal analysis are non-uniform due to the slab on the beam and the concrete blocks in the column. The flowchart in Fig. 7 (a) details the transient 2D-thermal analysis of the framework beam-slab and column-blocks sections subjected to non-uniform temperature fields.

The procedure starts with the input of the history-time curve of the gas temperature, the mixed-section geometry data (Fig. 7(b,c)), the temperature-dependent material properties, the Boltzman constant, the convection-radiation data, the time step Δt, and the total simulation time (*ts*). The mixed-section domain is discretized with PLANE-35 elements, and the transient thermal analysis is solved with Ansys. Finally, the full thermal response in the mixed-section is obtained at each time step, i.e., the time-history results of the temperatures and the thermal gradients (horizontal and vertical) in each of the finite elements of the mixed-section mesh. The horizontal and vertical thermal gradients are expressed with YY and ZZ, respectively, to relate them to the local directions of the structural beam finite element used in mechanical modeling (see Fig. 10).

Since concrete elements in the framework only fill an insulating role, only the thermal response in steel-section is considered at the end of the heat transfer analysis. Therefore, finalized the thermal analysis of the mixed-section in Fig. 7(a), the procedure continues at to calculate the three time-varying average components described in Fig. 2, i.e., the time-history results of the average temperature and thermal gradients (horizontal and vertical) in steel-section. Before starting these calculations, temperature and gradient results in the steel-section are selected.

The flowchart in Fig. 8 details the methodology by which the three constituent components of the section temperature profile (in Fig. 2) are obtained. For each instant (*t*), the procedure starts from the steel-section elements thermal response obtained with the procedure detailed in Fig. 7(a). The flowchart begins with the entry of the number of PLANE35 elements (*ne*) of the steel-section. To calculate the average temperature and the two average gradients of the steel-section at each instant (*t*), a cycle controlled by the counter (*i*) is performed, which counts the number of elements (*ne*) of the steel-section ($i = 1$ to *ne*). In this cycle, the elemental temperatures and gradients YY and ZZ obtained from the transient thermal analysis are stored in the variables Temp(*i*), Grad_YY (*i*), and Grad_ZZ(*i*), then, they are accumulated in the variables Sum_Temp, Sum_Grad_YY and Sum_Grad_ZZ. Once the cycle is finished, the average temperatures and gradients of the steel-section are calculated, dividing each summation updated value by the number of elements (*ne*). The values of the averages are stored in (Avg_Temp), (Avg_Grad_YY),

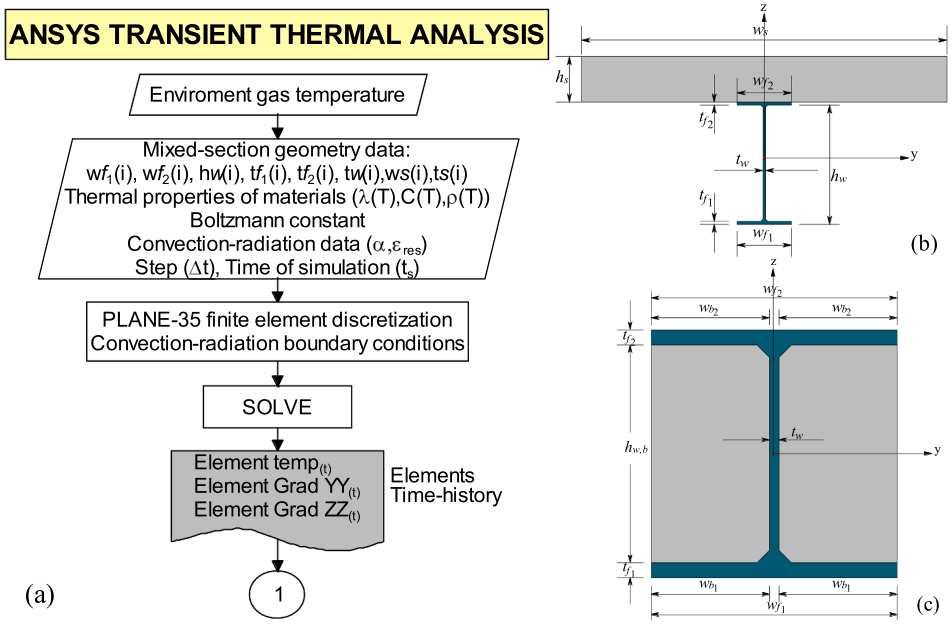

Fig. 7. Transient heat-transfer analysis flowchart of a mixed-section.

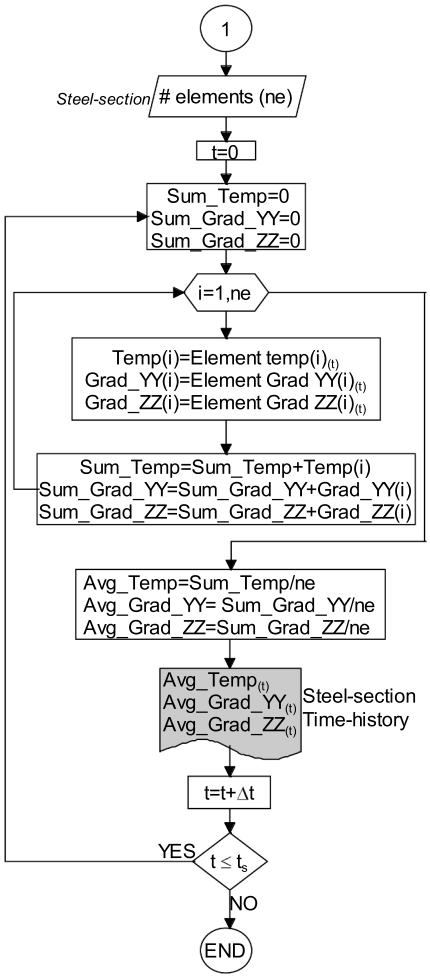

Fig. 8. Methodology for non-uniform temperature approach in a steel-section.

(Avg_Grad_ZZ) for each time (t). The process is repeated for each time ($t + \Delta t$) up to the total simulation time (ts). In the end, the complete tabulations of the three history-time curves of average temperature, average YY gradient, and average ZZ gradient are obtained. The procedure is applied for each steel-section of the structural member considered. In the present case study, the number of sections analyzed is two, the beam steel-section, and the column steel-section. In the flowchart in Fig. 8, the number of PLANE35 elements in the beam steel-section is $ne = 244$ and $ne = 278$ for the column steel-section.

6. Structural analysis of the framework

Since concrete only plays an insulating role in the framework, it only participates in the thermal resistance and not in the structural response; Therefore, the mechanical properties of concrete are not considered, only those of steel.

The real stress–strain ratio (σ-ε) of steel at high temperatures and the reduction factors $k_{y,\theta}$, $k_{p,\theta}$ and $k_{E,\theta}$ given by the EN 1993-1-2 standard, were used [29]. The yield stress of 408 MPa, the elastic modulus of 210 GPa, and the constant Poisson ratio of 0.3 were taken from [22]. The Creep effect on the deformation of steel was considered implicit in the material model. The Ansys model multi-lineal isotropic hardening with temperature dependence was used, which can adequately represent the stress–strain relationships of steel with temperature (based on Dounas and Golrand described in [31]). Variations of thermal expansion (α) of steel with temperature were also determined according to EN 1993-1-2 [29].

The thermal deformations introduced with thermal expansion (α) are very important in the mechanical analysis of the framework. Thus, the non-uniform field of temperature developed in the framework members sections by fire-action makes the material highly heterogeneous, resulting in additional bending deformations that increase with temperature.

In the Ansys structural analysis, geometric nonlinearity is activated to introduce the formulations of large deformations and deflections (GMNA). The convergence criteria for the solution of the nonlinear equations systems of the Newton-Raphson methods are defined. As concrete slabs and blocks only provide thermal insulation, they are not modeled in the structural analysis. The Cardington experiment reported that the joint remained intact and at lower temperatures than those measured at the beam and columns during the test; thus, the beam-column joint is considered rigid. The mechanical behavior of the half Cardington framework was modeled in 2D and 3D. Fig. 9 shows half of the steel 2D-framework idealization considering the symmetry. In the 2D-model, XY-plane-frame restraints were included in all nodes; additionally, the axial translation in the *x*-global axis and the rotation around the *z*-global axis at the beam mid-span were restrained considering the symmetry conditions; translations in the *x-global* and *y-global* directions were also restrained at the column bottom-end. Since the beam-finite element used for the modeling is 3D, translations in *z-global* direction (out-of-plane) were restrained in all nodes in the 2D-model. A bilinear spring with a nonlinear force-translation behavior was modeled at the position shown in Fig. 9 to represent the secondary framework constraint [27]. In 3D-model, XY-plane-frame restraints were released; additionally, symmetry condition at the beam mid-span remained (that means, only translation in the *y-global* direction was allowed). Also, full-translations and rotations about *x,y-global* directions were restrained at the column bottom-end in the 3D-model.

The Timoshenko-3D BEAM189 element was used to model the beam and column of the steel framework. This finite element is quadratic (three nodes), with seven degrees of freedom at each node (3 translations, 3 rotations about the *x*, *y*, *z-global* directions, and the warping magnitude to represent the cross-section deformations due to high temperatures (see Fig. 10 (a)). Each section of the BEAM189-finite element is a predetermined set of nine node cells with four integration points per cell (Fig. 10(b)). The number of cells influences the accuracy of the geometric and material properties and the ability to model the nonlinear stress–strain relationship in the element cross-section. The calculations of the material inelastic behavior and the section temperature variation are performed at the section integration points. The element supports uniform temperatures and thermal gradients that vary linearly in both cross-section directions and throughout the element [32]. BEAM189 has a great capacity for static and dynamic nonlinear analysis, including geometric and material nonlinearity, suitable for solving stability problems (buckling, post-buckling, and collapse). The

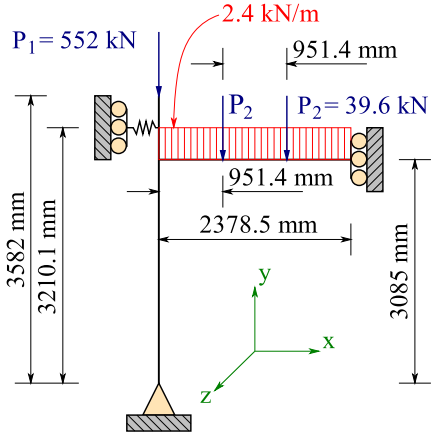

Fig. 9. Idealized Cardington framework.

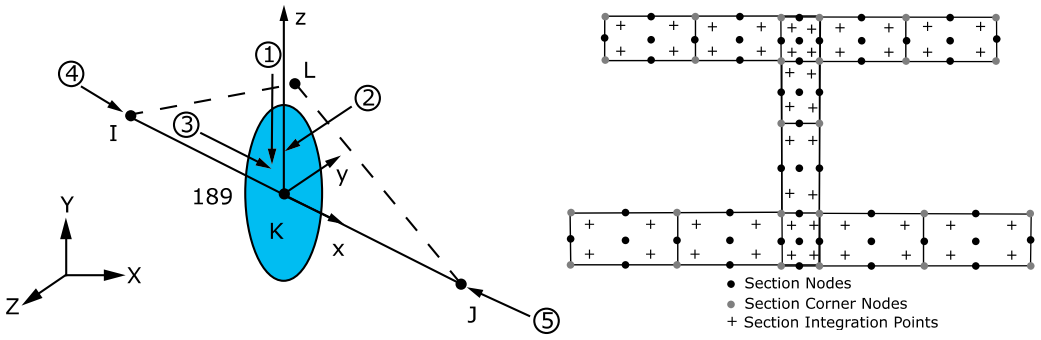

Fig. 10. BEAM189 definition and pseudo-mesh [32].

Timoshenko theory of the BEAM189 element assumes a shear-state in the cross-section (not present in Euler-Bernoulli theory). This assumption better approximates the cross-section deformation in deep beams considering the great relevance of shear effects in beams of heterogeneous material such as this case study [33]. As BEAM-189 is a three-dimensional finite element, some results can be calculated into the section's pseudo-mesh nodes, allowing for some post-processing results and extruded view. Results querying in extruded view are based on the post-processing query strings that interact with the database of the calculation results in the pseudo-mesh nodes of the section. This 3D-BEAM189 computing power allows the implementation of the proposed methodology.

Fig. 10(a,b) show the geometry, the nodes, the coordinate system (local and global), and the cross-section of the BEAM189-finite element. The meshing of the steel-beam and column cross-sections and the framework discretization with BEAM189 elements are shown in Fig. 11 (a,b). Half of the beam in Fig. 11(c) was discretized with five elements ($ne = 5$), and the column was discretized with ten elements ($ne = 10$).

Mechanical loads shown in Fig. 9 are applied at environment temperature and remain constant during the fire. The non-uniform temperature in the steel-section is applied through the three time-varying components previously obtained from the procedure in Fig. 8. Besides, a linear variation of temperature in the beam length is considered. The longitudinal variation of the temperature in the beam is included through reduction factors (fx) determined by a sinusoidal function that varies between 0.90 (at the beam/column connection) and 1.00 (at mid-span), considering that the fire location is at the beam mid-span [27,29]. Based on the discretization of the half beam (see Fig. 11(c)), the reduction factors (fx) calculated at the mid-point of each BEAM189-element are shown in Table 1. Fig. 12 shows the approximation of the longitudinal temperature variation in half beam discretized with the five BEAM189 elements ($ne = 5$).

The factor (fx) at the midpoint of each BEAM189-element is multiplied by the average component of temperature (T_{avg} in Fig. 2(b)) to include the beam temperature longitudinal variation, as shown in Fig. 12. As the average temperature component applied to the BEAM189 section varies in time, the temperature in beam length also varies in time.

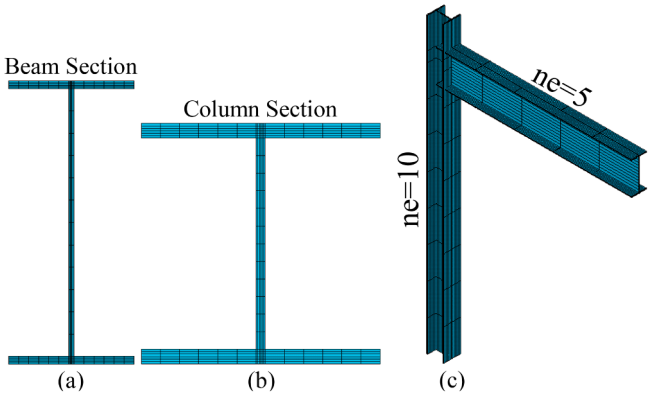

Fig. 11. Sections pseudo-meshing and BEAM189-framework discretization.

Table 1
Temperature variation factors along the beam.

	Relative distance	Length (mm)	Angle (x) (rad)	$fx = \sin(x)$
Connection→	0.0	0	1.120	0.900
	0.1	237.85	1.165	0.919
	0.3	713.55	1.255	0.951
	0.5	1189.25	1.345	0.975
	0.7	1664.95	1.435	0.991
	0.9	2140.65	1.526	0.999
Midspan→	1.0	2387.50	1.571	1.000

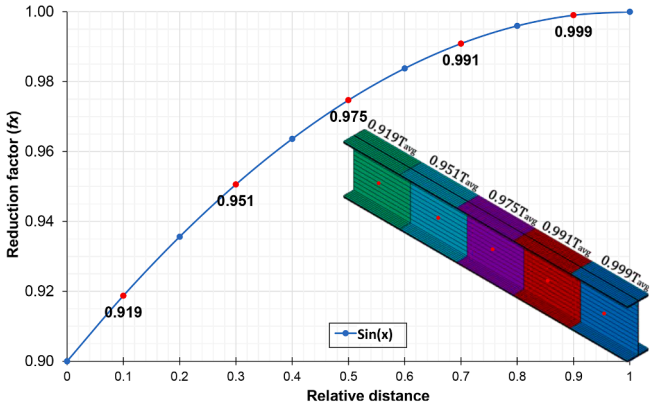

Fig. 12. Longitudinal temperature variation in half beam.

The structural analysis under fire can be approached using a static pseudo-time scheme or a dynamic real-time scheme, including a quasi-static time integration method. In this methodology, a static pseudo-time scheme is used because the aim is to find the structure's fire resistance time and the structural response to this failure time, so a static analysis is enough for this purpose. However, the methodology can be used in explicit or implicit dynamic analysis introducing the appropriate command sequences. Fig. 13(a) shows the mechanical analysis flowchart, in which the average temperature and average thermal gradients results of the steel-section at each time obtained from the procedure illustrated in Fig. 8 are applied in the BEAM189-section. Therefore, this approach can consider the different heterogeneous material behaviors produced by temperature changes in the section in time. This methodology can approximate the non-uniform temperature field in beam-type elements and is useful for rigorously analyzing steel frames under fire,

saving modeling and calculation times.

In the mechanical analysis in Fig. 13 (a): i) the structural members are the beams and columns; ii) each structural member has a single section (the member is prismatic over the entire length); iii) the geometric and material properties are assigned to each section, the section is assigned to each member, and loads are assigned to each BEAM189-finite element that discretizes the member; iv) all BEAM189-finite elements have a single section; v) the members are grouped by section, and the elements are grouped by member. In this way of working, as in object-oriented programming, heritages are transferred among objects, in this case, among sections, members, and elements.

The analysis is defined through loops controlled by next control variables: the pseudo-time (t), the number of sections counter (i), the counter of the members' number with the same section (j) and, the counter of elements number of each member grouped by section (k). The limits of these control variables are respectively: the pseudo total

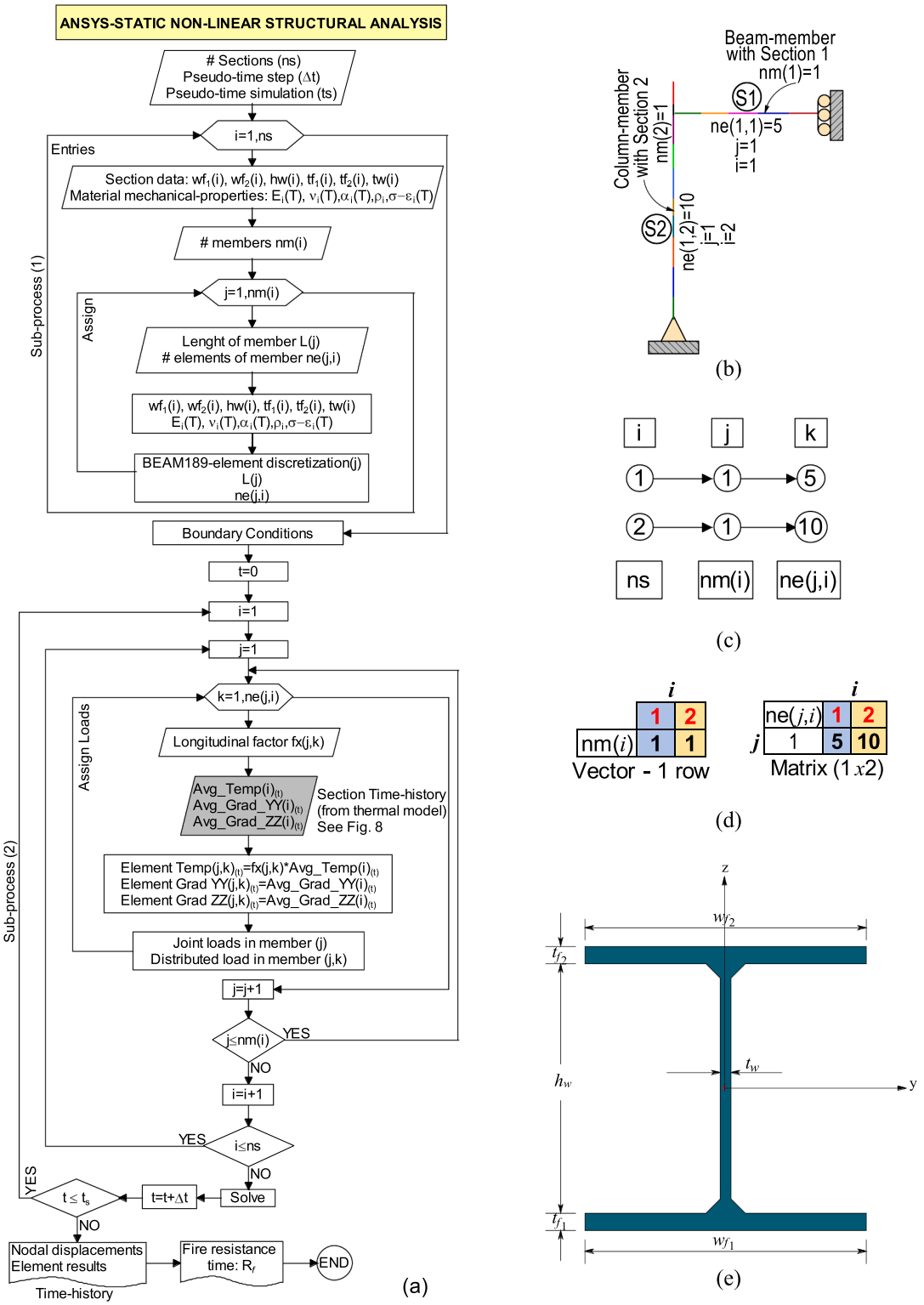

Fig. 13. Mechanical analysis flowchart.

simulation time (*ts*), the number of sections (*ns*), the number of members (*nm*(*i*)) in the same section (*i*), and the number of BEAM189-elements (*ne*(*j*,*i*)) that discrete the member (*j*) with section (*i*). The number of sections (*ns*) controls the entire process since the section carries the nonlinearity of the material and the three components time-histories that approximate the non-uniform temperature field. In general, *nm*(*i*) is a size vector (*ns*), and *ne*(*j*,*i*) is a matrix dimensioned from the largest number of members with the same section and the number of sections (>nm(*i*),*ns*).

In this case study, there are two sections (*ns* = *2*) -Section 1 corresponding to the beam and Section 2 corresponding to the column-, so the loop controlled by the counter (*i*) goes from 1 to 2 (*i* = 1,2). The number of members with Section 1 (beam cross-section) is *nm*(1) = 1, and the number of members with Section 2 (column cross-section) is *nm*(2) = 1, so the highest number of members with the same section is 1, and the cycle controlled by the counter (*j*) goes from 1 to 1 (*j* = 1 to 1) for each section run. Therefore, the largest number of members with the same section is 1 (>nm(*i*) = 1). The number of elements in Member 1 (beam) with Section 1 is *ne*(1,1) = 5 and the number of elements in Member 2 (column) with Section 2 is *ne*(1,2) = 10. The application of the procedure in the analyzed framework is detailed in Fig. 13(b), the relations between the variables are shown in Fig. 13(c), and the matrix forms of the variables *nm*(*i*) and *ne*(*j*,*i*) are presented in Fig. 13(d).

E.g., in an entire Cardington framework model (3 members: 1 beam and 2 columns; 2 sections: Section 1 for the beam, Section 2 for the columns), the number of members with Section 1 is *nm*(1) = 1, and the number of members with Section 2 is *nm*(2) = 2, so the largest number of members with the same type of section is 2, and they have the section named Section 2. The counter (*j*) for Section 1 goes from 1 to 1 (*j* = 1 to 1), and for Section 2 the counter (*j*) goes from 1 to 2 (*j* = 1 to 2). The number of elements in the member with Section 1 is *ne*(1,1) = 10 (beam), the number of elements in the first member having Section 2 is *ne*(1,2) = 10 (column 1), and the number of elements in the second member having Section 2 is ne(2,2) = 10 (column 2). Fig. 14(a-c) illustrate the handling of the variables, the vector *nm*(*i*), and the matrix *ne*(*j*,*i*), respectively, when analyzing the entire framework.

The analysis procedure in Fig. 13(a) starts with the next entries: the number of sections in the structure (*ns*), the definition of the pseudo time step (Δ*t*), and the total pseudo-time of the simulation (*ts*). The term pseudo-time refers to the static analysis incremental control that solves geometrical and material nonlinearity without the inertial effects of the dynamic schemes controlled by the real-time parameter [34].

The sub-process (1) starts with the section data entries through a loop controlled by the section's counter (*i*). In this loop (*i* = 1 to *ns*), for each section, geometrical data (w_{f1},w_{f2},h_w,t_{f1},t_{f2},t_w, shown in Fig. 13(e)), the temperature-dependent material mechanical properties, and the number of members *nm*(*i*) with the same section (*i*) are entered. Then, through another loop (*j* = 1 to *nm*(*i*)), each member (*j*) in section (*i*) is assigned: the member length L(*j*), the number of BEAM189-finite elements *ne*(*j*,*i*) that discrete the member, the section dimensions, the material properties, and the discretization are performed with BEAM189 elements. After assigning the boundary conditions to the model nodes according to the analysis dimension (2D or 3D) and the symmetry conditions, the sub-process (2) is started to assign the loads on the elements through a loop controlled by the elements counter (*k*) of each member (*j*) in section (*i*). In this loop (*k* = 1 to *ne*(*j*,*i*)), the three components that approximate the non-uniform temperature field and the mechanical loads are assigned to each element (*k*). The reduction factor *fx*(*j*,*k*) is applied to each element (*k*) to discretize the longitudinal temperature variation. The uniform temperature component (Element Temp(*j*,*k*)) is the average section temperature (Avg_Temp(*i*)) multiplied by the factor *fx*(*j*,*k*), and the other two gradient components (Element Grad YY(*j*,*k*)) and (Element Grad ZZ(*j*,*k*)) are the average section gradients (Avg_Grad_YY(*i*)) and (Avg_Grad_ZZ(*i*)) respectively. Once the non-uniform temperature components have been applied, the uniform load on each element (*k*) and the nodal loads are applied. The sub-process (2) is carried out for each pseudo time (*t*) through nested loops controlled by the control variables (*i*), (*j*), and (*k*). Loops continue while the loads are assigned in all of the elements, and the nonlinear static analysis is performed for each pseudo-time step (Δ*t*) up to the total pseudo simulation time (*ts*). Finally, the time-history results of the nodes displacements and the results in the elements are obtained.

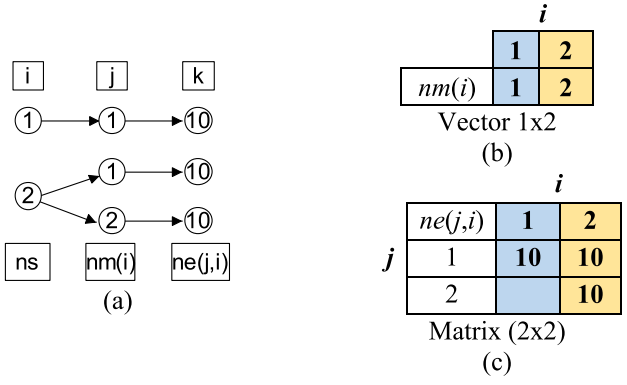

Fig. 14. Handling of variables: case of the entire framework.

7. Thermal results of sections

Thermal results are temperatures and thermal gradients in the beam and column sections. In this case, the temperature is given by a field, T (Y,Z,*t*), so at each point (Y,Z) in a section, the two-dimensional field of the thermal gradient (TGy,TGz) shows the direction of temperature rises. In contrast, the temperature gradient's magnitude determines how fast the temperature rises in that direction. The thermal gradient is directed from lower to higher temperatures. The gradient vector module is proportional to the temperature change per unit of length, °C/mm (e.g., large vectors of thermal gradient correspond to those areas where the temperature changes quickly).

Figs. 15 and 16 show the temperature time-histories at three points (two on the flanges and one on the centroid indicated by the numbers 1, 2, 3) for the beam and column steel-sections. The temperature results at the three points obtained from the Ansys-heat transfer models (described in Fig. 7) compare very well with those of Franssen *et al.* and Santiago *et al.* done in Ceficoss, Safir, and Abaqus available in [18,22,27]. The temperature curves in the beam section top flange point and the column section web point are the lowest due to the concrete slab thermal insulation effect in the beam and concrete blocks in the column. Fig. 15 shows changes in the cooling speed at points 1 and 3 of the beam section. After 25 min, the web cools faster than the top flange because the gas surrounding the web cools faster than the concrete slab on the beam top flange. The above shows that in the heating stage, the concrete insulating elements reduce the heat transfer to the steel section, and in the cooling stage, they reduce the heat dissipation speed in those places of the section where steel and concrete are in contact. The outer flange in the column has lower temperatures than the inner flange; therefore, the shadow effect is verified. This non-uniform temperature behavior influences the mechanical behavior of the framework.

Fig. 17(a) and 18(a) show temperature isocontours in sections (including the concrete elements) at the end of the test (*t* = 30 min). In Fig. 17(b) and 18(b), the temperature isocontours in the steel-sections more clearly show the temperature variation in the two directions, demonstrating the non-uniformity of the steel section temperature field. There is an apparent symmetry in the horizontal distribution that is not present in the vertical distribution. The web temperature profiles show the thermal insulation due to concrete elements and the shadowing effect on the column outer flange. Since the sections are not heated uniformly around their perimeter, internal thermal gradients along the local ZZ axis (Fig. 17(c) and 18(c)) are important. E.g., the concrete slab

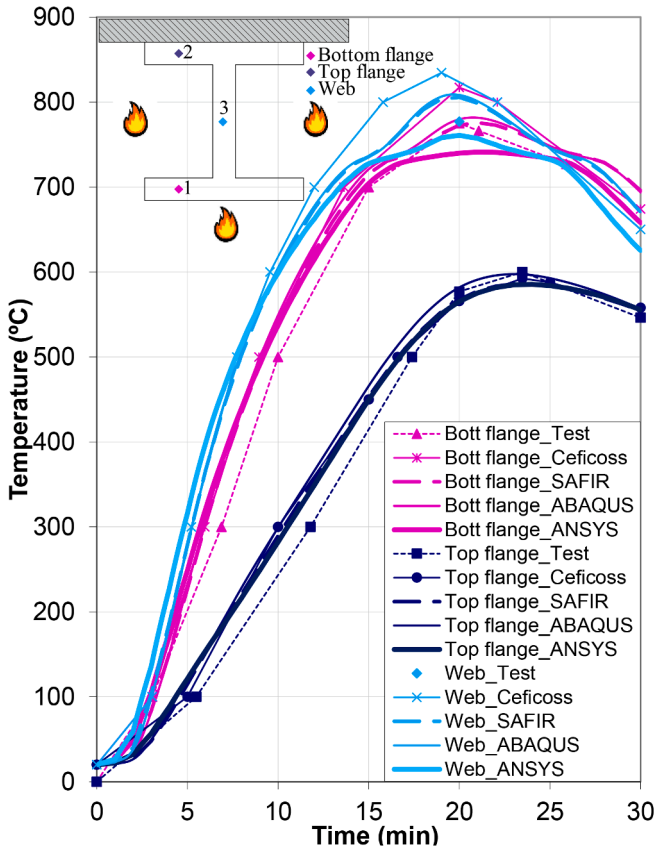

Fig. 15. Temperature at three points on the beam steel-section.

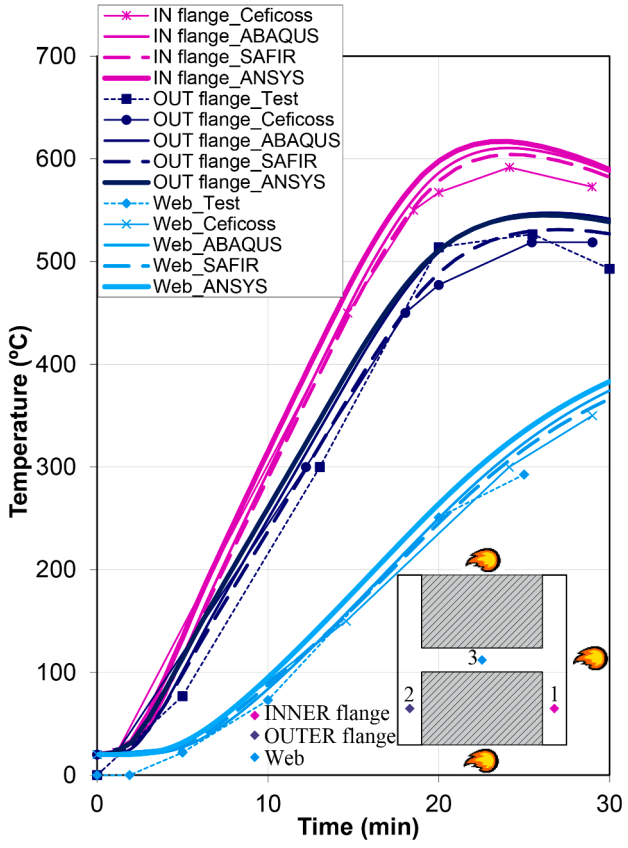

Fig. 16. Temperature at three points on the column steel-section.

creates non-uniform heating of the beam that causes the temperature drop towards the slab (Fig. 17(c)), so an approximation of the temperature distribution in the beam section with a linear variation is adjusted. However, the column section non-uniform heating created by the concrete blocks causes the web to maintain lower temperatures than the flanges and the temperature in the section increases from the center of the web to the flanges. The shading effect on the outer face and the exposure to the inner face fire establish two temperature variations in the section, one that goes from the web center to the outer flange and another that goes from the web center to the inner flange. Therefore, the temperature distribution approximation in the column with a single linear variation can influence the prediction of the column lateral displacement; despite this, an approximation of the temperature distribution in the column section with a linear variation is acceptable (see Fig. 25). Horizontally (local YY-axis), the temperature variations are lower, so an approximation of linear variation in that direction is justified.

In Fig. 17(c), the gradient sign on the entire web is negative; this means that the temperature increases from top to bottom in the Z-axis' negative direction as expected (see Fig. 17(b)). Similarly, in Fig. 18(c), the gradient sign on the web is negative in the bottom-middle and positive in the top-middle since the temperature increases from the center to the web ends. That means the temperature increases in Z-axis's negative direction in the bottom-middle and Z-axis's positive direction in the top-middle, as expected (see Fig. 18(b)). In beam and column sections, it can be seen: 1) the highest gradient values are at the ends of the web (just at the fillet), where the temperature values change more rapidly than other parts of the section, 2) in both flanges the gradient slope changes because of the gradient intensity becomes decreasing.

Fig. 19 shows the horizontal and vertical thermal gradient isocontours in the beam steel-section for three representative times (5, 15, and 30 min). Fig. 20 shows the horizontal and vertical thermal gradient isocontours in the column steel-section for three representative times (5, 20, and 30 min). The two gradients show an initial upward behavior. The beam gradients grew up to about 15 min and in the column up to about 20 min. Then, they begin to decrease until an almost uniform distribution of temperatures exists towards the end of the test ($t = 30$ min).

Thermal gradients are element results and are located at the centroid of each PLANE35-element. Figs. 19 and 20 isocontours are the smoothed results of the sections' thermal gradients in the indicated times. In these results, small localized areas are observed (denoted by MN (minimum) and MX (maximum)) where the gradients achieve relative values that are high (positive or negative) and which indicate large temperature changes in a small region of the section. These are shown, e.g., in Fig. 19 (e), where there are small zones where the vertical gradient ZZ in the steel beam section achieves a minimum value MN of −5.87 °C/mm and a maximum gradient MX of 1.34 °C/mm. Also, in Fig. 20(b), there are small horizontal gradient zones YY in the steel column section where the MN gradient is −2.65 °C/mm, and the MX gradient is 2.64 °C/mm. Figs. 19 and 20 show simultaneous positive and negative gradient values, which tend to balance out, resulting in almost zero positive or negative values.

Meanwhile, Fig. 21(a-b) show the average thermal gradient histories of the steel sections in the beam and the column, where most of the time, the resulting gradient is negative, indicating that the temperature decreases in the direction of the concrete slab in the beam and, the direction of the outer flange in the column due to the shading effect. In Fig. 21(a-b), average thermal gradients are not constant in time, and their behavior is different in the heating and cooling phases. Fig. 21(a) shows that thermal gradients magnitude increases and decreases in the heating and cooling stage, respectively, i.e., gradients magnitude increases from start fire up to 15 min in the beam section and 17 min in the column section; then, gradients magnitude decreases until the end of the fire. Hence, knowing the gradients' behavior in the whole fire scenario is important mainly for the subsequent three-dimensional analysis of post-

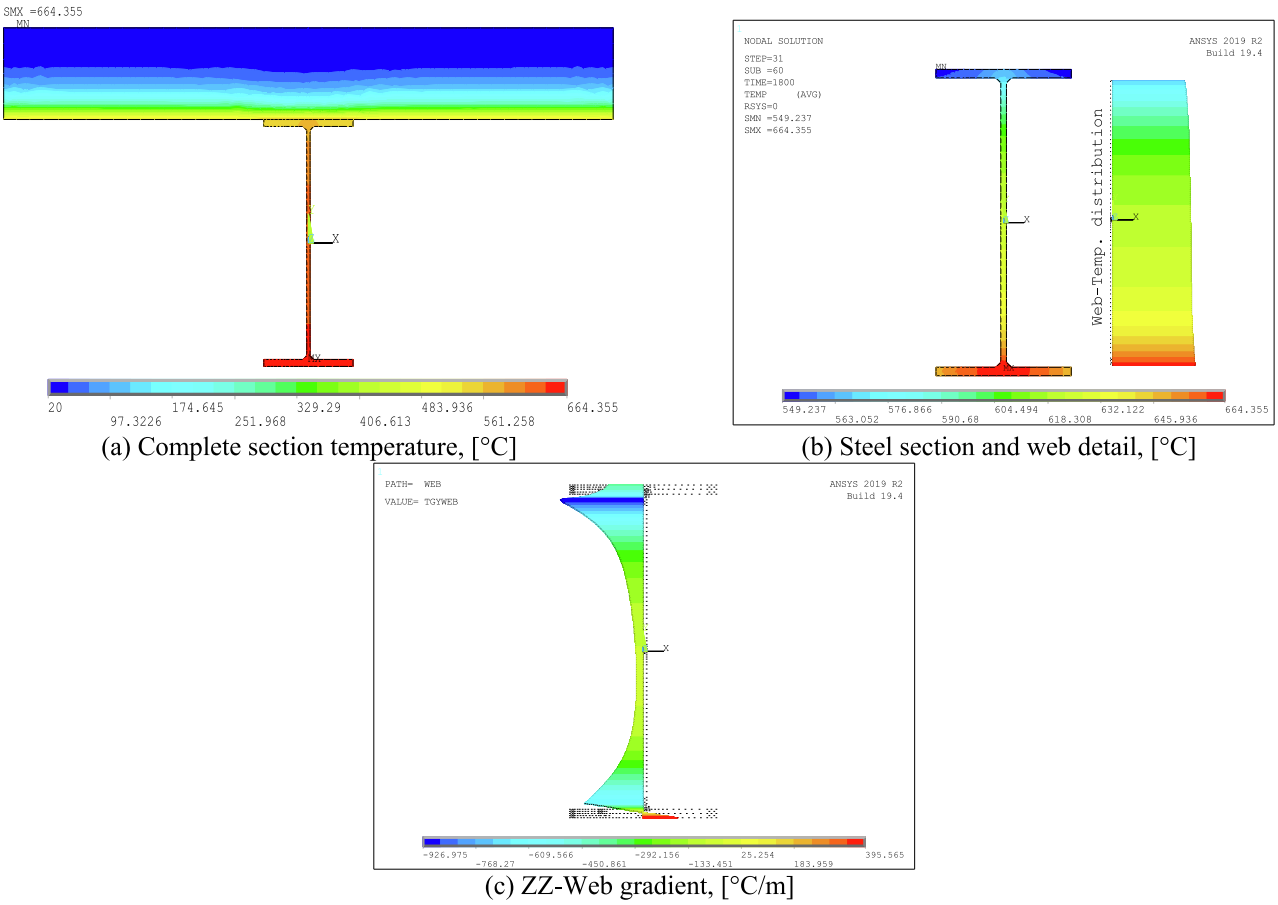

(a) Complete section temperature, [°C]

(b) Steel section and web detail, [°C]

(c) ZZ-Web gradient, [°C/m]

Fig. 17. Temperature isocontours and ZZ-thermal gradient in the beam section at t = 30 min.

buckling or collapse, which can occur in the cooling phase [35].

In Fig. 21(a), the average ZZ gradient values (in the web) of the beam section are higher due to the asymmetry of the section in the vertical direction: $\langle \frac{\text{concrete}}{\text{steel}} \rangle$, while the low average gradient values YY are due to the section symmetry in the horizontal direction: $\langle \text{steel} | \text{steel} \rangle$ on the bottom flange, and $\langle \frac{\text{concrete}}{\text{steel}} | \frac{\text{concrete}}{\text{steel}} \rangle$ on the upper flange. The average ZZ gradient values (in the web) of the column section are lower than those of the beam because of the concrete blocks between the flanges that protect the web from the high fire temperatures.

In Fig. 21(b), the horizontal average gradient values YY in both sections show a more uniform behavior. They are lower than the vertical ones, with the maximum horizontal average gradient value being one-seventh of the absolute maximum vertical average gradient value in the beam and half in the column. Although the horizontal average gradient values YY are similar in both sections, it takes only 5 min for the beam to get the maximum value. In comparison, the column takes 15 min to get the same value. In both sections, the values of horizontal average gradient YY are lower than those of vertical average gradient ZZ; however, it was confirmed that horizontal gradients are indispensable in approximating the section non-uniform temperature distribution. Not including them creates problems of non-convergence of the solution. In Fig. 21(a), the vertical gradient peaks ZZ in the beam and column sections are presented at $t = 15$ and $t = 17$ min, respectively. It can be seen that when the gradient is maximum, inflection points occur in the deflection curves of the beam and column where the deflection rate increases (see Fig. 24). This drop in the average values of the ZZ gradients is due to two considerations: i) the drop in the gas temperature in the compartment from $t = 15$ min (see Fig. 5) and ii) the decrease in the steel thermal conductivity with the temperature.

Fig. 22(a,b) show for the three points on the flanges and the web centroid of the beam and column sections (indicated by numbers 1, 2, and 3) the temperature histories calculated in the thermal model against temperature histories applied in the structural model using the proposed methodology. Temperatures applied at these points (for each time) are approximated by Eq. (1). According to this equation, the average section temperature is applied at the centroid where gradients are null, so that, at the centroid, the temperature applied is the average section temperature. Fig. 22(a,b) show the average temperature histories $T_{avg}(t)$ at the centroid of the beam and column sections used in the methodology for the approximation of non-uniform section temperature. Although these average temperatures are applied at the centroid, the $T_{avg}(t)$ curve is not compared with the calculated temperature curve at the centroid in the thermal model because they have different meanings. I.e., the average section temperature applied at the centroid represents the uniform temperature component used to approximate the temperature applied at one point of the section in the structural model, which no-match the centroid temperature calculated in the thermal model. Besides, the temperature time-history curves calculated in the thermal model and those applied in the structural model (at the two points of the flanges) do not match; that is because the applied temperature field using the average temperature and the two average gradients of the section are approximations that balance the over and under errors in the section domain at each time step.

By approximating the non-uniform temperature distribution in the section (which is a curved surface in space) through an average oblique plane, points of temperature above and below the plane (major over-heated in some cases and major under-heated in others) are located that balance the result in each time step. Fig. 23 shows this situation for a time $t = 15$ min in the beam section and for a time $t = 20$ min in the column section. In these two figures, the temperature curved surfaces

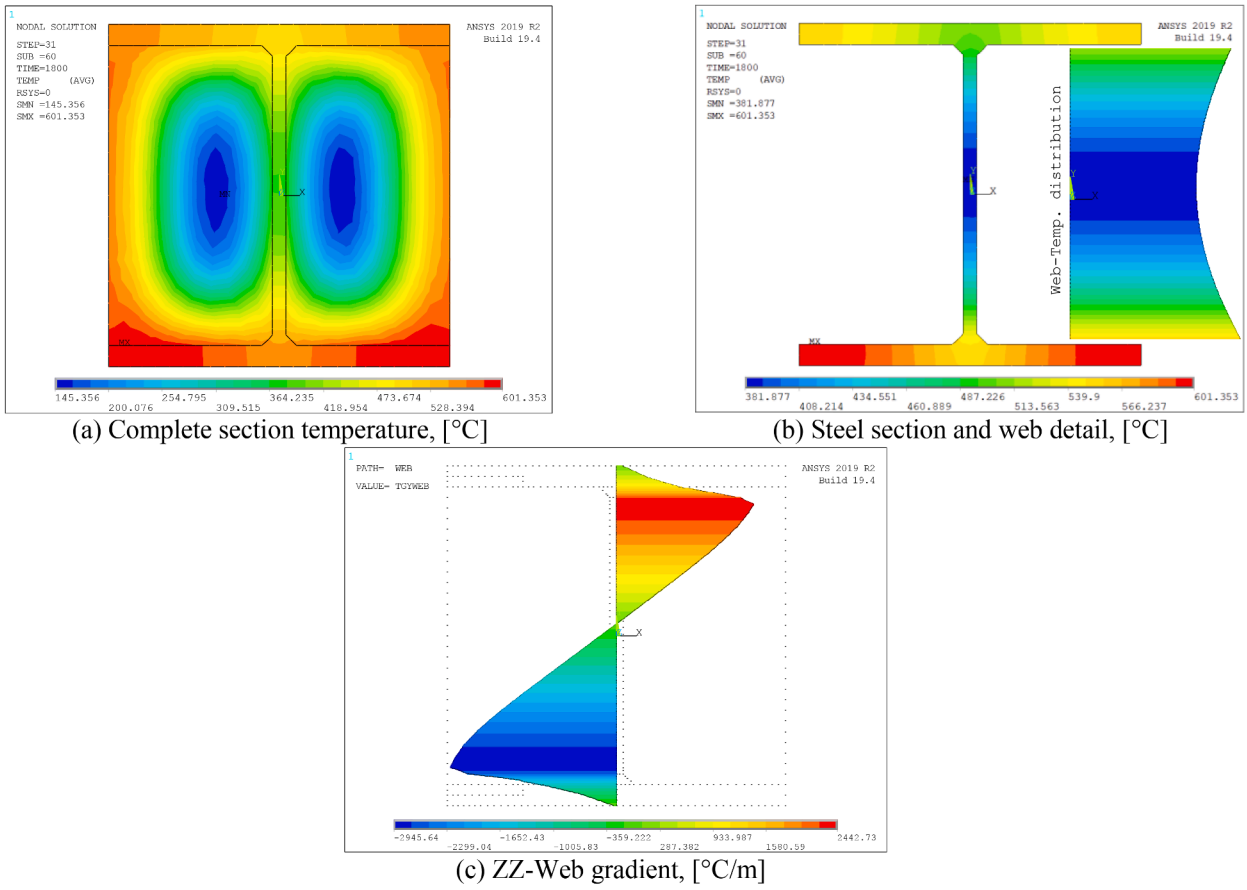

(a) Complete section temperature, [°C]

(b) Steel section and web detail, [°C]

(c) ZZ-Web gradient, [°C/m]

Fig. 18. Temperature isocontours and ZZ-thermal gradient in the column section at t = 30 min.

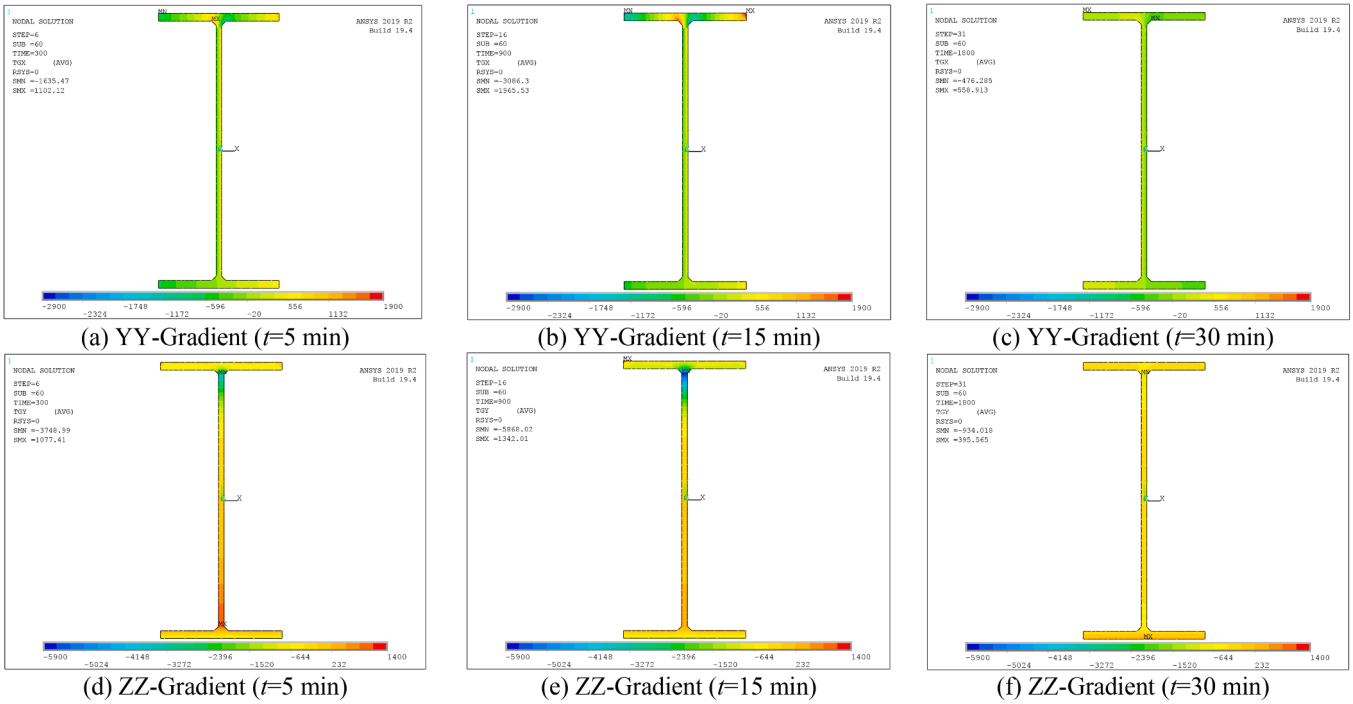

(a) YY-Gradient (t=5 min)

(b) YY-Gradient (t=15 min)

(c) YY-Gradient (t=30 min)

(d) ZZ-Gradient (t=5 min)

(e) ZZ-Gradient (t=15 min)

(f) ZZ-Gradient (t=30 min)

Fig. 19. Isocontours of YY-horizontal gradient and ZZ-vertical gradient in the I-profile section of the steel beam, in °C/m.

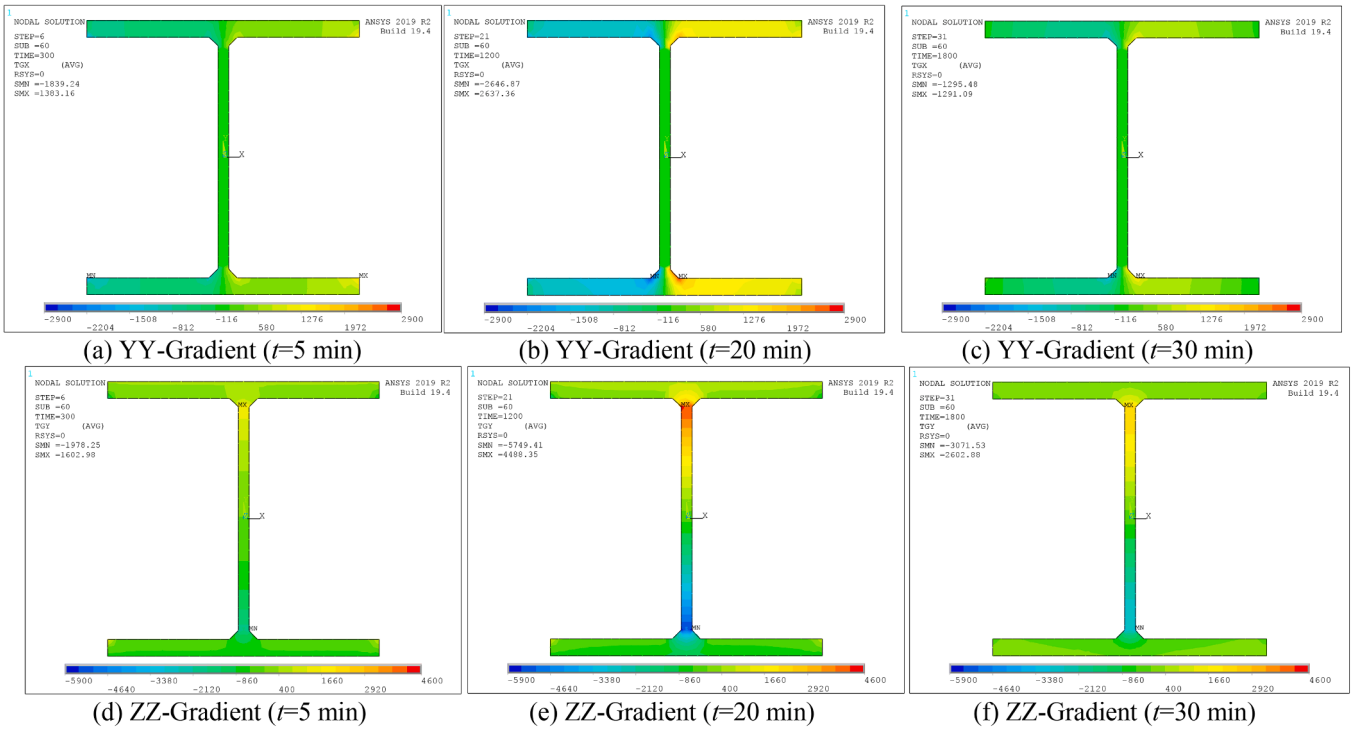

Fig. 20. Isocontours of YY-horizontal gradient and ZZ-vertical gradient in the I-profile section of the steel column, in °C/m.

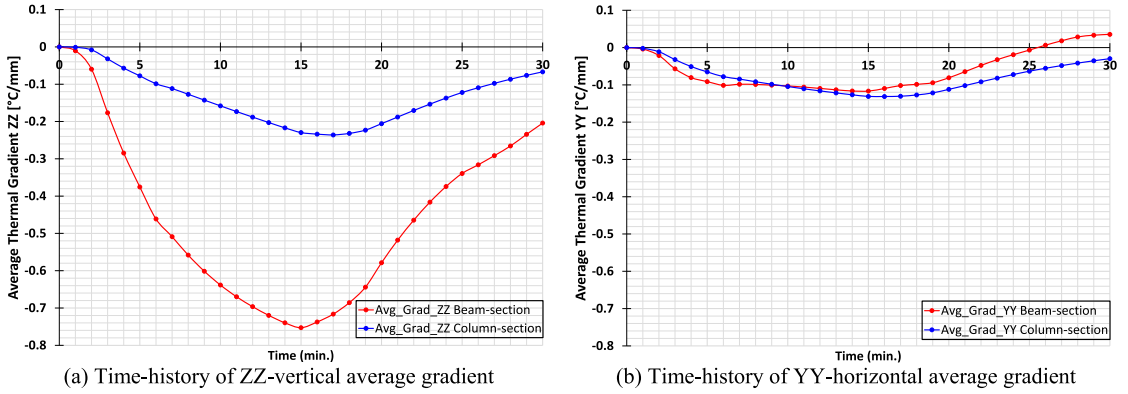

(a) Time-history of ZZ-vertical average gradient (b) Time-history of YY-horizontal average gradient

Fig. 21. Average transversal gradient time-histories in the steel sections of the beam and column.

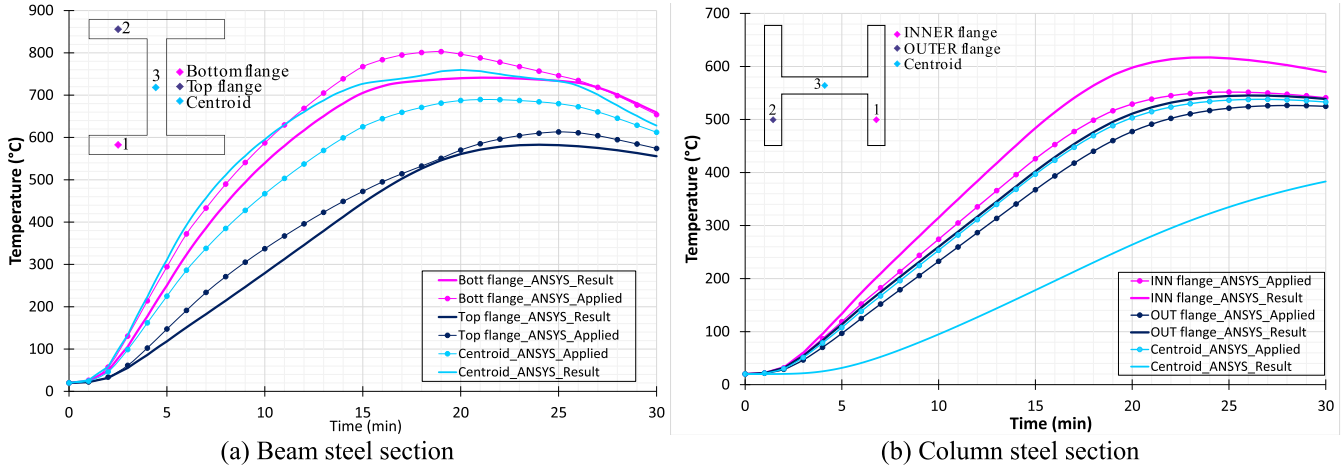

(a) Beam steel section (b) Column steel section

Fig. 22. Time-histories of average temperatures calculated and applied at three points in the sections.

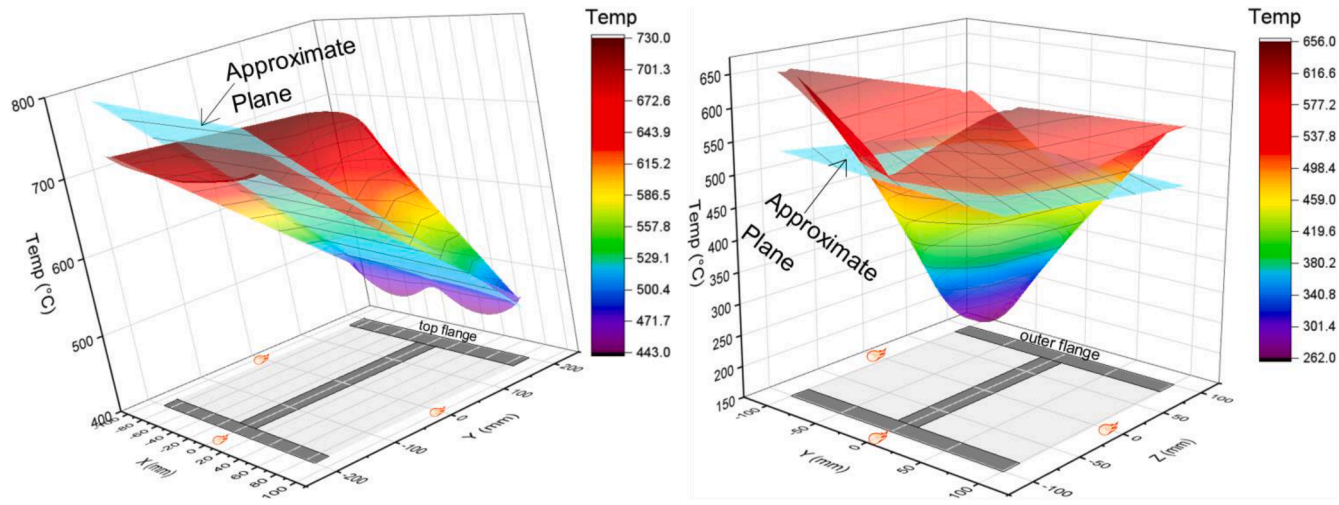

(a) Beam steel section (t=15 min) (b) Column steel section (t=20 min)

Fig. 23. Calculated temperature surfaces and applied approximate temperature planes.

from the thermal model calculations and the average temperature planes used in the methodology to approximate the non-uniform temperature in the structural model sections are represented. On the surfaces, the isocontours indicate the temperature values, and the surface slopes represent the thermal gradients.

E.g., in the beam section (Fig. 23(a)), the high slope of the temperature surface at the web reproduces the high vertical gradient value in the Z-direction. In contrast, the low slopes at the flanges denote the low horizontal gradient values in the Y direction. In the column section (Fig. 23(b)), high slopes are observed over the flanges and the web that mean high values of the horizontal and vertical gradient in the Y and Z directions, being larger the gradients in the web. This situation is verified by the gradient distributions in Fig. 19(b,e) on the beam and 20(b,e) on the column. On the other hand, the result of the approach-plane cut in the temperature surface explains the temperature balance. Above means, in the centroid of the section, the plane height is equal to the average section temperature, and the slope of this plane in each direction (Y and Z) coincides with the values of the average gradients (horizontal and vertical) of the section. E.g., in the beam section (Fig. 23(a)), the Z-direction slope approaching-plane is higher than the Y-direction slope. In the column section (Fig. 23(b)), the slopes of the temperature approaching plane in the two directions (Y and Z) are more similar to each other because of the section symmetry. The highest average gradient values are in the Z-direction and the lowest in the Y-direction. The temperature surfaces are useful insofar as they allow the influence of boundary conditions on the section to become evident. E.g., when comparing Fig. 23(a,b), it is observed that the influence of the radioactive shadow on the steel thermal gradient (in the column) is less than the concrete boundary condition effect (in the beam).

8. Framework's mechanical results

In this work, three different mechanical models have been done to validate and verify the proposed methodology:

- A 2D model with the spring shown in Fig. 9, whose calibration allows representing the bending of the beam-column assembly properly. This 2D model was done to verify the 2D simulations of the experiment carried out by Santiago et al. available in [22].
- A 3D model with the same spring as the 2D model mentioned above. This model is necessary to check 3D effects such as section warping and flexural–torsional buckling that can appear in frames at elevated temperatures and cannot be captured with 2D models.
- A springless 3D-model for evaluating the influence of the subsidiary framework lateral resistance on the three-dimensional fire response of the framework.

The validation of the proposed methodology is carried out based on the following results of: (a) the Cardington test, which are included in the Latham *et al.* report [25,26], and (b) the 2D-numerical simulations of the experiment carried out by Santiago *et al.* [22]:

- Maximum deflection in midspan beam.
- Lateral displacement at column mid-height.
- Column end extension.
- Fire resistance time.

Lateral displacement at column mid-height and column end extension are both new analyses that make it possible to validate the proposed methodology and take advantage of the 3D-modeling capabilities using 3D-beam finite elements.

Fig. 24 (a) compares the experimental beam mid-span deflections with those obtained by Santiago *et al.* [18,22] and the three mechanical models proposed. It is observed that all models make a good prediction. Safir results match those of the Ansys-3D models up to about the 16th minute. The 2D-model, on the other hand, is closer to results given by Ceficoss and Abaqus. Fig. 24(b) compares only the lateral (central) displacements at half the column height obtained with the different programs. All deflection predictions are in the centroid. It can be seen again that the results obtained with all of the models are similar.

Fig. 25 compares the lateral displacement at column mid-height measured by the extensometer (located about a quarter of the outer flange width: $¼w_f$) with those obtained from the Ansys-3D models. Deflection predictions are obtained outside the centroid at the extensometer position located on the column's outer face.

It is observed that, in the first 16 min, the calculated deflections are higher than measured, probably because the approximation of linear variation of the temperature in the section does not completely represent the bi-laminate effect. This effect is the curvature produced by expanding the heated inner face when the section perimeter temperature is not uniform. The bi-laminate effect in the column, in turn, produces a balancing of internal forces by the temperature that makes the deflections in the column laterally smaller, as observed in the measurements of the experiment. However, it is essential to note that from 17 min (the same time of the average vertical gradient peak ZZ, see Fig. 21(a)) and until the final failure time, the prediction of lateral displacement of the column is very close to the experiment (in the

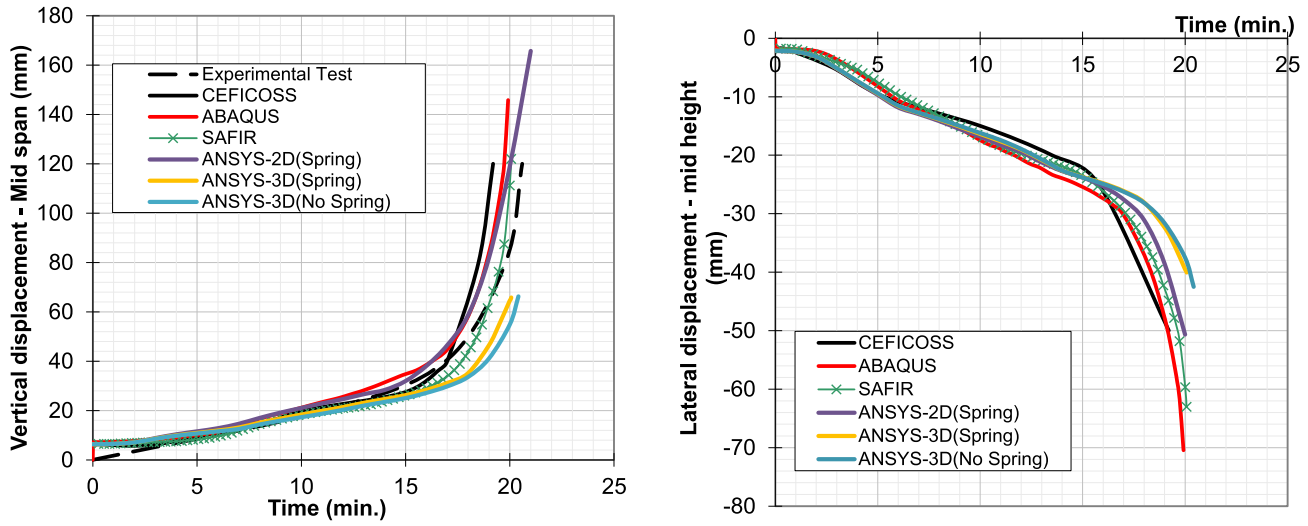

(a) Max. vertical displacement - beam midspan (b) Lateral displacement - column mid-height

Fig. 24. Deflection comparison of the framework members (centroidal results).

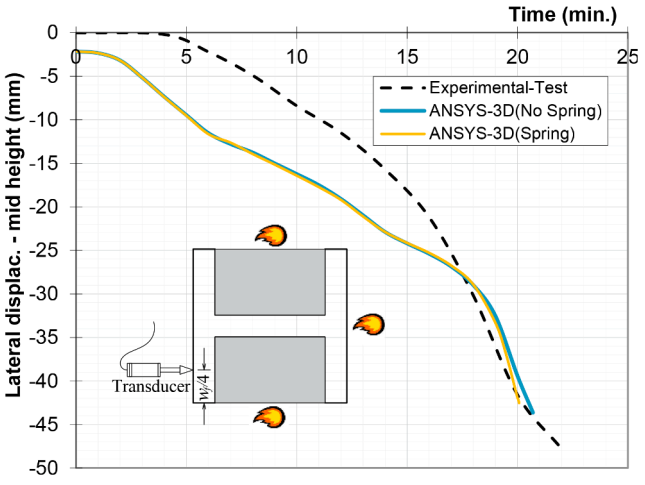

Fig. 25. Lateral displacement - column mid-height, (¼w_f).

cooling zone, see Fig. 5).

Fig. 26(a,b) show the lateral displacements at mid-height of the column at three points located on the outer face in the Ansys-3D models at t = 20 min. The 39.43 mm model prediction without spring (in the extensometer position, indicated in red color) compares very well with the 41.6 mm reported in the experiment. If the spring is included, the prediction slightly increases to 41.3 mm, closer to the experiment value. These non-centroidal results are calculated into the pseudo-mesh nodes of the BEAM189 element section. Results querying in the nodes of the finite element outer face (in extruded view) are possible by interaction with the results' database in the pseudo-mesh nodes of the section.

Table 2
Time of fire resistance (R_f).

Numerical model	R_f	Ratio (Num./Exp.)
Ceficoss	19′12″	0.93
Safir	20′04″	0.97
Abaqus	19′51″	0.96
Ansys-2D (Spring)	21′00″	1.02
Ansys-3D (Spring)	20′44″	0.97
Ansys-3D (No Spring)	20′28″	0.99

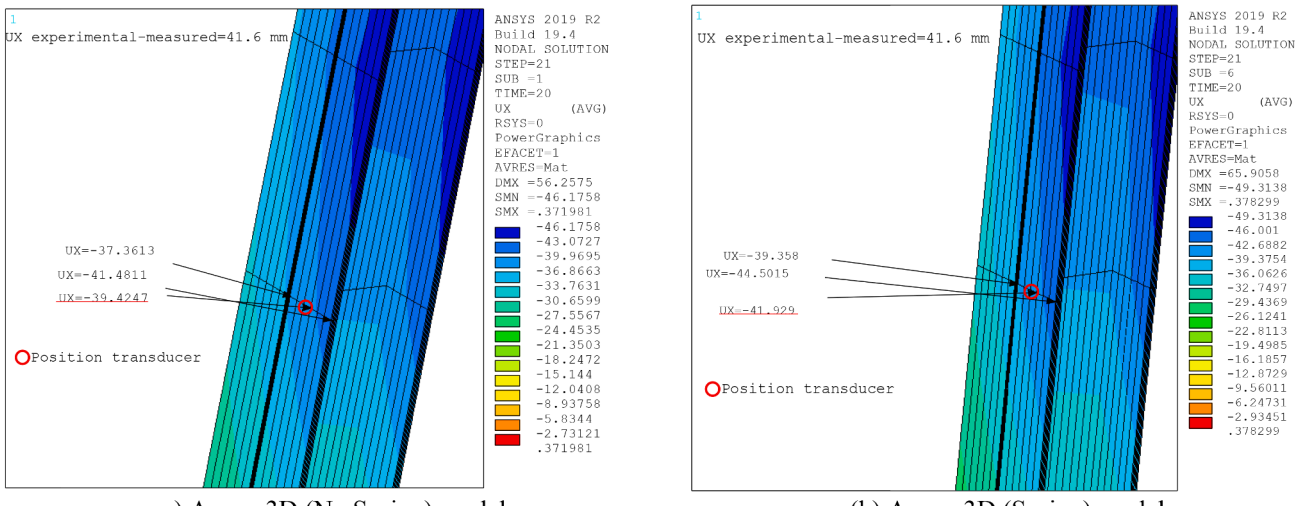

a) Ansys-3D (No Spring) model (b) Ansys-3D (Spring) model

Fig. 26. Lateral displacement on outer face (w_f/4) - column mid-height (t = 20 min), in extruded view.

Table 2 shows the fire resistance time according to the simulations carried out by Santiago *et al.* [18,22] and by the authors with the new methodology implemented in Ansys. The results are compared with the fire resistance time of 20′36″ reported in the test. It is observed that the Ansys-3D (No Spring) model gives the best prediction, although the results are similar for all the structural models.

Finally, Table 3 shows the CPU time for the three models built in Ansys using parallel distributed memory-MPI calculation in 6 physical cores on a Dell Mobile Workstation 7530/64 bits, Intel Xeon Processor-2.71 GHz, and Ram-32 GB. Despite the high nonlinearities present, the results show that CPU times are low in the three models (less than 1 min).

From the analysis carried out, the capacity of the three models developed in Ansys with the strategy presented in this paper to correctly predict the response of the framework with a low computational cost is concluded. Considering that the two framework 3D-models' deflections predictions are practically the same, the following results focus on analyzing the Ansys-3D (No Spring) model results as it is the model that includes 3D-phenomena that better approximates the failure time and has the smallest CPU cost.

Fig. 27 shows the vertical deflection predictions at two points in the middle and corner top end of the outer flange (column end extension). The test report exactly no-specified the extensometer position, so it was assumed from the photographic evidence it was the midpoint. Both predictions show similar behavior to that measured in the experiment. The 20.68 mm calculated in the middle flange at $t = 20$ min is closer to the 20.6 mm measured in the experiment. At the outer end of the flange, the calculated value is 22.04 mm. The differences between the measured and simulated values depend on the experimental measurement point location as the section is rotated.

A detail of the extruded column end is shown in Fig. 28. The colors of the vertical displacement isocontours ($t = 20.47$ min) at the end of the column indicate the section rotation (differential displacements at all of the section points are not constant). This situation affects the measurement of vertical deflection.

Fig. 29 shows the lateral column deflections (UZ) perpendicular to the plane of the framework. Deflections are calculated at the mid-height and the top end of the column. Initially, the values are small, and as time goes by, when the material weakens by fire, sectional warping and buckling appear, which can compromise the column stability. Some oscillations and startles are observed in small fractions of time at the final times, allowing some instability to be inferred. The UZ values in the mid-height of the column are positive, and those at the top-end are negative, indicating inflections.

Fig. 30 shows the applied temperature distribution to the frame ($t =$ 20.47 min) using the non-uniform temperature approximation in the sections and the temperature reduction factors in the beam length. The different colors indicate the different temperature values in the sections and along the beam. With these temperature loads properly applied in space and time through the proposed methodology, mechanical results are obtained reasonably adjusted to the structural response measured in the laboratory (see Figs. 24 to 27). The applied temperature values (806 °C in the beam and 605 °C in the column) are in accordance with the maximum temperatures calculated in Figs. 15 and 16.

Fig. 31(a) shows the 3D deformation of the frame. A buckling is identified in the column of greater intensity towards the end t of the test. In the front view (Fig. 31(b)), a flexural–torsional buckling is also observed in the column, which can only be seen when the complete framework response is modeled in 3D. The structural response shows that the non-uniform temperature field in sections and elements affects the structure displacement field in all of the three dimensions.

Fig. 32 shows the three-dimensional displacement field presented in the framework by the simultaneous action of applied loads, the deformations due to non-uniform temperatures, and buckling phenomena due to high temperatures. The following reasons can cause the latter: i)

Table 3
Calculation time for Ansys models.

Numerical model	CPU Time (sec)
Ansys-2D (Spring)	27.000
Ansys-3D (Spring)	40.625
Ansys-3D (No Spring)	32.938

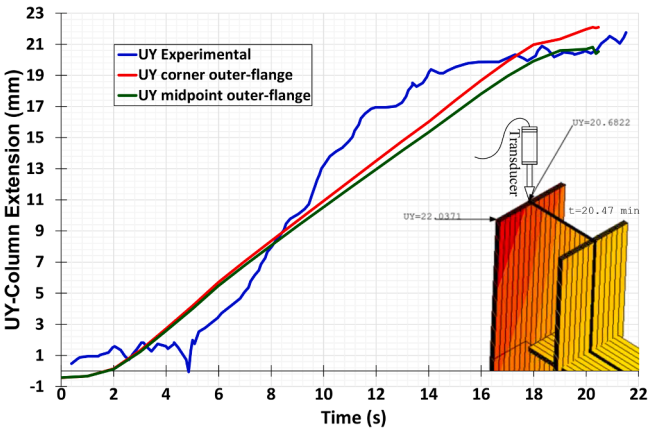

Fig. 27. Column end extension in two points (t = 20.47 min).

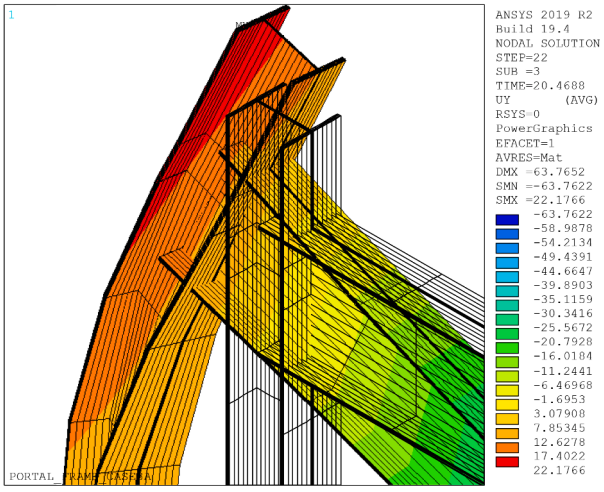

Fig. 28. UY-displacements in the column end (t = 20.47 min), in extruded view.

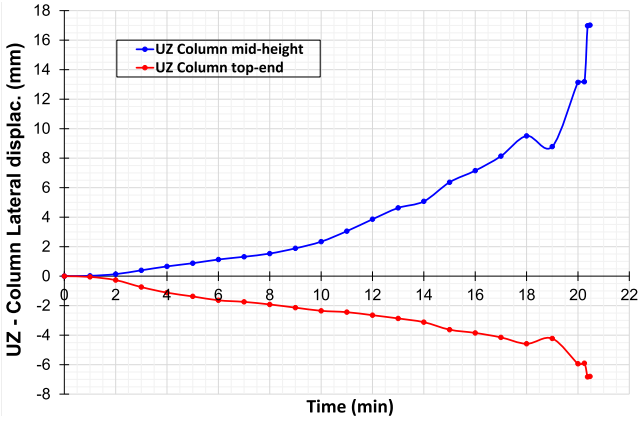

Fig. 29. Normal column displacement (t = 20.47 min).

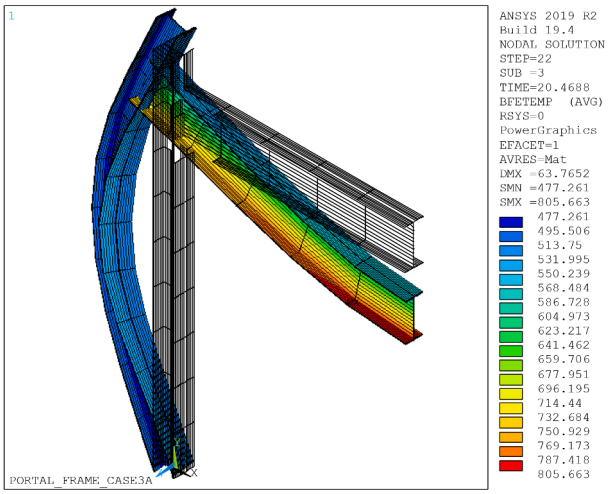

Fig. 30. Non-uniform temperature applied (t = 20.47) min), in extruded view.

the weakening of the material, ii) imperfections or second-order phenomena (instability because of large deformations which appear due to considerable differences between deformed and non-deformed shape) and, iii) the coupling of the displacements because of heterogeneity created in the material by the internal thermal gradients (under the fire action, each cross-section becomes composed of a large number of different materials due to the different mechanical features which occur at each temperature, at each time and each point of the section [36]). In Fig. 32(a-f), it can be seen that all the degrees of freedom vary within the section of the elements, confirming that the displacement field is 3D. The different column rotations in the three global directions, *x*, *y*, *z*, demonstrates a biaxial stress state. In this case study, two bending planes are generated (produced by moments, buckling, flexural-torsion buckling, warping, and temperature), which cannot be considered when the frame is modeled for a 2D-displacement field.

Important displacements originated in the framework by the steel ductility and the thermal expansion cause a steel plasticization by the heat. Fig. 33(a,b) show the Von Mises plastic deformations produced by the action of mechanical loads and temperature loads (t = 20.47 min), respectively. It can be seen that the order of magnitude of the plastic deformations produced by mechanical loads and those created by temperature loads in the final fire resistance time is very similar. Approximately 50% of the framework plastic deformation is produced by mechanical loads and the other 50% by temperature loads. Consequently, temperature deformations are significant for calculating the framework deformation field and studying its mechanical behavior.

Results of warping, bicurvature and bimoment are important insofar as they allow inferring the presence of possible flexural–torsional buckling in places where large changes in the angle of torsion occur, suggesting zones of local instability in the members of the structure. Fig. 34 shows the warping behavior in the frame (t = 20.47 min). This effect is relevant as the open sections of the framework decrease the torsional stiffness with increasing temperature. Fig. 34(a) shows warping due to high temperatures, mainly in the column, verified with the bicurvatures and bimoments shown in Fig. 34(b,c), respectively. The influence of warping in the simulation is more remarkable in the column than the beam because there was no restriction to warping (since there were no point loads along the column). For stability considerations, warping had to be restricted towards the beam midspan (due to the applied loads), precisely where the beam distortions were significant, according to the experiment. Solvers with greater capacity to overcome the convergence problems caused by the instability resulting from the high fire nonlinearity are necessary to get better results from the beam warping.

The torsional rotation results, warping, bicurvature, and bimoment are related to each other and make sense when analyzed together. I.e., since warping is the first derivative of torsional rotation, the zero-warping point is where the maximum torsion occurs (in the column, it is between the positive and negative warping points). This condition is verified in the middle zone of the column when Fig. 32(e) and 34(a) are compared. Similarly, being the bicurvature, the first derivative of the warping and the bimoment a function of the bicurvature, the two points of maximum and minimum value of warping present in the column (Fig. 34(a)) match the points of zero bicurvature shown in Fig. 34(b). The bicurvature is significant at the column middle and upper zones where the lateral bending is registered (see Fig. 31). The column positively twists in the middle of the column and negatively at the end. Bicurvature signs indicate changes in the direction of twisting along the column. The almost constant values of bimoment in the central zone of the column in Fig. 34(c) just in the region where the bicurvature is maximum (between the positive and negative warping) suggest that in this region, the rotated sections no longer present large relative changes of position or shape between them.

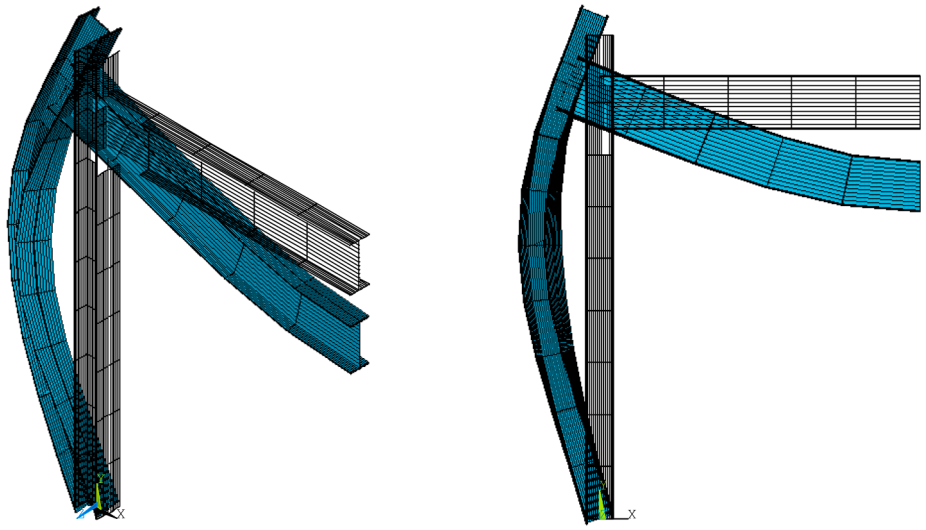

(a) Deformed-isometric view (b) Deformed-frontal view

Fig. 31. Flexural-torsional buckling (t = 20.47 min), in extruded view.

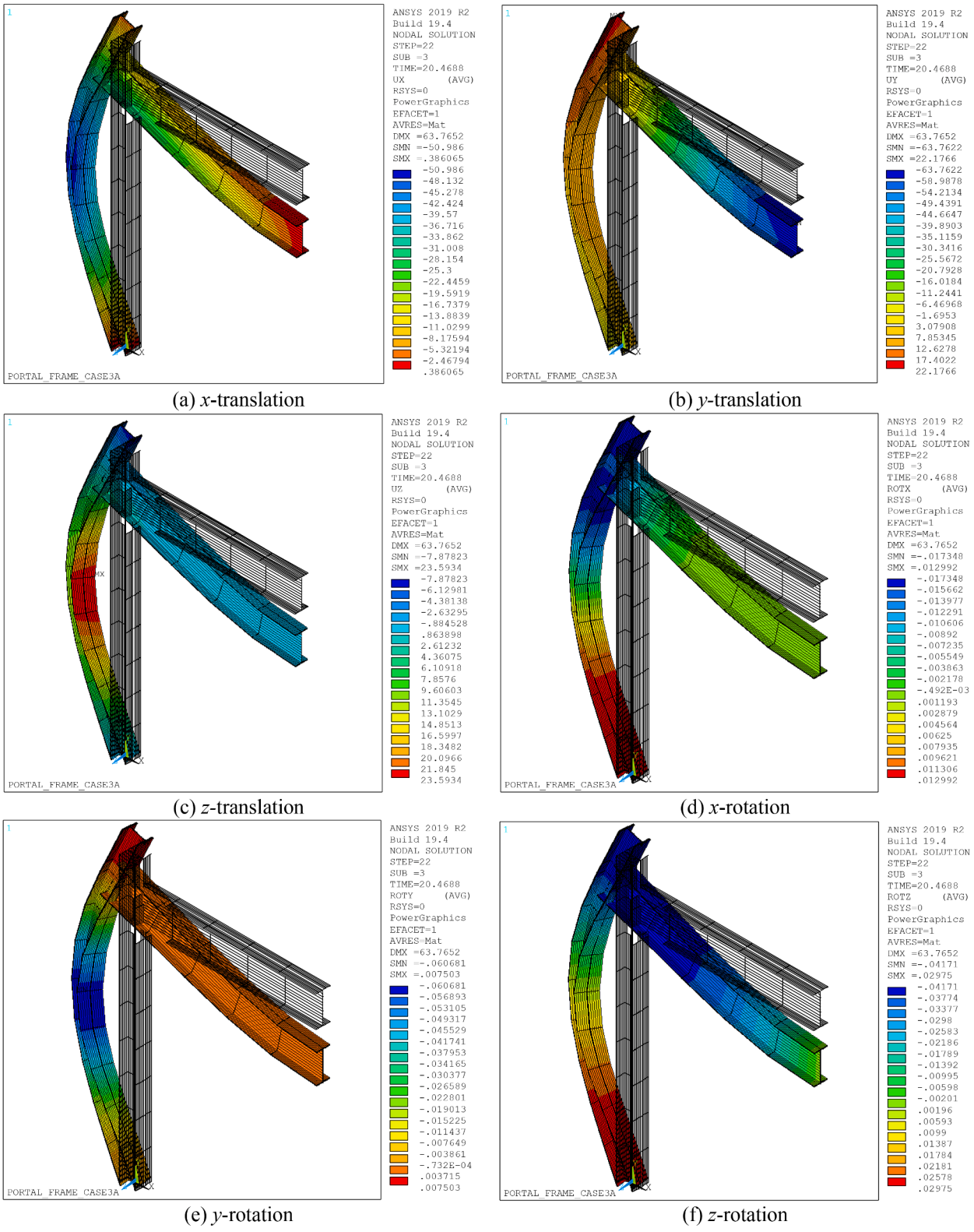

Fig. 32. 3D-displacement field isocontours (t = 20.47 min), in extruded view.

9. Conclusions

This paper proposes a new methodology to represent the effects of non-uniform heating in structures subjected to fire action. The procedure is based on using beam-type finite elements with the Timoshenko formulation and the temperature field representation through an average value of the temperature and the section thermal gradients. The methodology has been validated with results of the behavior (displacements) of the Cardington framework and the 2D numerical simulations of the Cardington experiment carried out by Franssen *et al.* and Santiago *et al.* [18,22,27]. The following conclusions can be drawn:

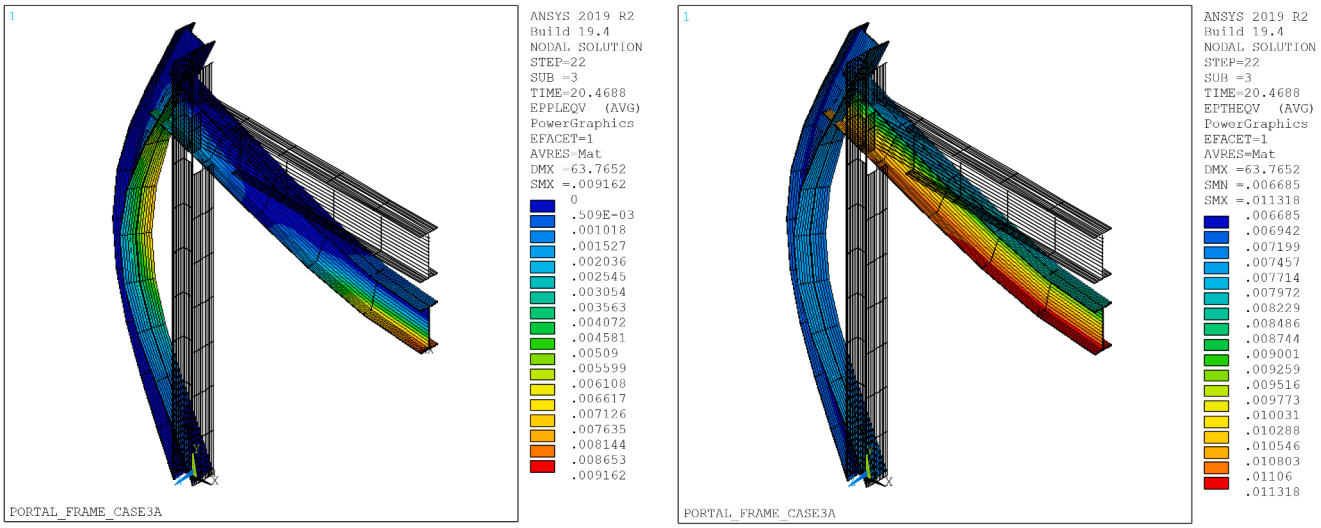

(a) Plastic deformation due to mechanical load (b) Plastic deformation due to temperature load

Fig. 33. Von Mises plastic deformations in the framework (t = 20.47 min), in extruded view.

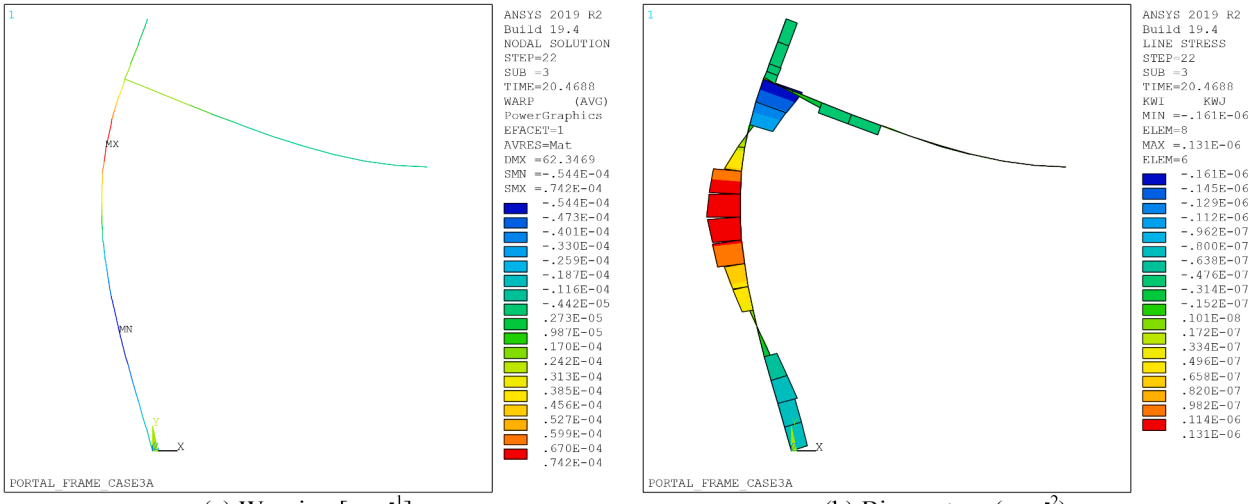

(a) Warping [mm^{-1}] (b) Bicurvature (mm^{-2})

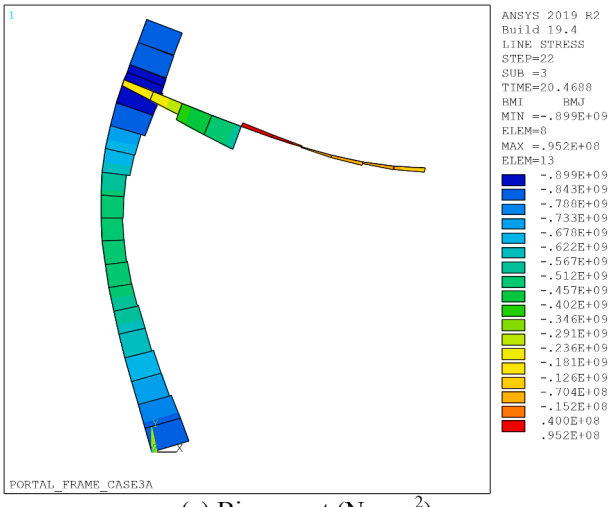

(c) Bimoment (N-mm^{2})

Fig. 34. Flexural-torsion effects in the framework (t = 20.47 min).

- In a fire situation, the insulating elements in the frame members (the slab on the beam and the blocks between the columns) accentuate the thermal gradients, causing the steel (being a homogeneous material at environment temperature) to behave like a highly heterogeneous material. The fire makes the sections behave as if they were composed of several materials due to the temperature dependency of steel mechanical properties. This heterogeneity -asymmetrical- caused by the temperature field -asymmetrical- in the section, originates from a coupling between the axial and bending effects. Therefore, an axial force produces a curvature, and a bending moment induces elongation of the members that affect the displacements field of the 3D-framework, favoring the appearance of displacements, rotations, and additional shearing effects, buckling and warping. These considerations justify Timoshenko's theory of the BEAM189 element in modeling the analyzed frame members. The above concludes that a good approximation of the mechanical structure response is determined by the type of beam element used to build the models.
- The proposed methodology is general, systematic, and enables the correct representation of a non-uniform and time-varying temperature field in the structure. These are significant advantages over other used strategies that represent the non-uniform temperature distributions from pre-established and constant relationships throughout the fire (e.g., the included in [17–20,22]).
- The methodology for determining the temperature field, including the variation of gradients in time, allows for 3D-structural analyses adapted to the 3D-nature of fire and the existence of non-uniform temperature fields in real structures.
- The non-uniform temperature field in the 3D- beam section calculated from the simulation results of the section heat transfer over the entire fire scenario makes it possible that structural effects in the cooling phase can also be modeled. Although in this Cardington framework experiment, only deflections were measured up to the fire resistance time (when the first failure occurs), it can be seen that from about 17 to 21 min, the framework structural effects in the cooling phase (of the gas) are being considered, e.g., buckling evidence in the column.
- The proposed methodology with 3D-beam elements correctly predicts the 3D-field of displacements and 3D-effects that appear in structures under the action of fire (buckling, flexural-torsion buckling, warping, and coupling). Therefore, the methodology avoids using more complex finite elements (shell or solid), simplifying the structural modeling, and reducing its cost (modeling time, memory, storage, and computer calculation time). All of this allows tackling nonlinear phenomena present in structures subjected to fire action easily. It means that the proposed methodology represents a significant step forward towards the generalized application of performance-based approaches to deal with the effects of fire on structures. By doing so, this methodology also opens the path for a wider application of probabilistic models to complex structures under fire.

Declaration of Competing Interest

The authors declare that they have no known competing financial interests or personal relationships that could have appeared to influence the work reported in this paper.

Acknowledgements

Thanks are due to the Fundación Carolina, the Universitat Politècnica de València, and the Universidad Surcolombiana for the support given to this research through the 2018-2019 Ph.D. scholarship.

References

[1] CTBUH. Tall Buildings in Numbers. The Global Tall Building Picture: Impact of 2019. CTBUH J Int J Tall Build Urban Habitat 2020:1–61.
[2] Shyam-Sunder S, Gann RG, Grosshandler WL, Lew HS, Bukowski RW, Sadek F, et al. Final Report on the Collapse of World Trade Center Building 7, Federal Building and Fire Safety Investigation of the World Trade Center Disaster (NIST NCSTAR 1A). Washington 2008.
[3] Shan S, Li S. Fire-induced progressive collapse mechanisms of steel frames with partial infill walls. Structures 2020;25:347–59. https://doi.org/10.1016/j.istruc.2020.03.023.
[4] Shakib H, Zakersalehi M, Jahangiri V, Zamanian R. Evaluation of Plasco Building fire-induced progressive collapse. Structures 2020;28:205–24. https://doi.org/10.1016/j.istruc.2020.08.058.
[5] Šulc S, Šmilauer V, Patzák B, Cábová K, Wald F. Linked simulation for fire-exposed elements using CFD and thermo-mechanical models. Adv Eng Softw 2019;131:12–22. https://doi.org/10.1016/j.advengsoft.2019.02.007.
[6] Horová K, Jána T, Wald F. Temperature heterogeneity during travelling fire on experimental building. Adv Eng Softw 2013;62–63:119–30. https://doi.org/10.1016/j.advengsoft.2013.05.001.
[7] Xu L, Zhuang Y. Storey-based stability of unbraced steel frames at elevated temperature. J Constr Steel Res 2012. https://doi.org/10.1016/j.jcsr.2012.06.010.
[8] Jacques L, Béchet E, Kerschen G. Finite element model reduction for space thermal analysis. Finite Elem Anal Des 2017;127:6–15. https://doi.org/10.1016/j.finel.2017.01.001.
[9] B.D. R, M. SK. Behaviour of steel columns with realistic boundary restraints under standard fire. Structures 2020;28:626–37. https://doi.org/https://doi.org/10.1016/j.istruc.2020.08.028.
[10] Alos-Moya J, Paya-Zaforteza I, Hospitaler A, Loma-Ossorio E. Valencia bridge fire tests: Validation of simplified and advanced numerical approaches to model bridge fire scenarios. Adv Eng Softw 2019;128:55–68. https://doi.org/10.1016/j.advengsoft.2018.11.003.
[11] Jeffers AE, Beata PA. Generalized shell heat transfer element for modeling the thermal response of non-uniformly heated structures. Finite Elem Anal Des 2014;83:58–67. 10.1016/j.finel.2014.01.003. https://doi.org/10.1016/j.finel.2014.01.003.
[12] Rigobello R, Coda HB, Munaiar Neto J. A 3D solid-like frame finite element applied to steel structures under high temperatures. Finite Elem Anal Des 2014;91:68–83. https://doi.org/10.1016/j.finel.2014.07.005.
[13] Alos-Moya J, Paya-Zaforteza I, Hospitaler A, Rinaudo P. Valencia bridge fire tests: Experimental study of a composite bridge under fire. J Constr Steel Res 2017;138:538–54. https://doi.org/10.1016/j.jcsr.2017.08.008.
[14] Peris-Sayol G, Paya-Zaforteza I, Alos-Moya J, Hospitaler A. Analysis of the influence of geometric, modeling and environmental parameters on the fire response of steel bridges subjected to realistic fire scenarios. Comput Struct 2015;158:333–45. https://doi.org/10.1016/j.compstruc.2015.06.003.
[15] Quiel E, Garlock ME, Paya-Zaforteza I. Closed-form procedure for predicting the capacity and demand of steel beam-columns under fire. J Struct Eng 2011;137:967–76. https://doi.org/10.1061/(ASCE)ST.1943-541X.0000443.
[16] Davidson MT, Harik IE, Davis DB. Fire Impact and Passive Fire Protection of Infrastructure: State of the Art. J Perform Constr Facil 2013;27. https://doi.org/10.1061/(asce)cf.1943-5509.0000295.
[17] Allam A, Nassif A, Nadjai A. Behaviour of restrained steel beam at elevated temperature – parametric studies. J Struct Fire Eng 2019;10:324–39. https://doi.org/10.1108/JSFE-11-2018-0036.
[18] Santiago A, Haremza C, Simões da Silva L, Rodrigues JP. Numerical behaviour of steel columns subject to localized fire loading. In: Topping BH V., Costa Neves LF, Barros RC, editors. Proc. Twelfth Int. Conf. Civil, Struct. Environ. Eng. Comput., Stirlingshire, Scotland: Civil-Comp Press; 2009.
[19] Burges I, Alexandrou M. Composite beams. In: Ed. Wald F, Burgess I, Kwasniewski L, Horová K, Caldová E, editors. Benchmark Stud. Verif. Numer. Model. fire Eng. 1st ed., Prague: CTU Publishing House; 2014.
[20] Burges I, Alexandrou M. Steel beams. In: Ed. Wald F, Burgess I, Kwasniewski L, Horová K, Caldová E, editors. Benchmark Stud. Verif. Numer. Model. fire Eng. 1st ed., Prague: CTU Publishing House; 2014.
[21] Burgess I, Plank R, Shephered P. Vulcan 2019.
[22] Santiago A, Haremza C, Lopes F, Franssen JM. Numerical behaviour of steel columns under localized fire loading. In: Ed. Wald F, Burgess I, Kwasniewski L, Horová K, Caldová E, editors. Benchmark Stud. Exp. Valid. Numer. Model. fire Eng. 1st ed., Prague: CTU Publishing House; 2014.
[23] Kumar S, Miles S, Welch S, Vassart O, Zhao B, Lemaire AD, et al. EUR 23200 - Integrating advanced three-dimensional modelling methodologies for predicting thermo-mechanical behaviour of steel and composite structures subjected to natural fires. Luxembourg: Office for Official Publications of the European Communities; 2009.
[24] Rackauskaite E, Panagiotis K, Rein G. Model parameter sensitivity and benchmarking of the explicit dynamic solver of LS-DYNA for structural analysis in case of fire. Fire Saf J 2017;90.. https://doi.org/10.1016/j.firesaf.2017.03.002.
[25] Latham DJ, Thomson G, Kirby BR, Wainman DE. Second natural fire test on a loaded steel frame at Cardington. Rotherham 1986.
[26] Cooke GME, Latham DJ. The inherent fire resistance of a loaded steel framework. Steel Constr Today 1987;1:49–58.
[27] Franssen JM, Cooke GME, Latham DJ. Numerical simulation of a full scale fire test on a loaded steel framework. J Constr Steel Res 1995;35:377–408. https://doi.org/10.1016/0143-974X(95)00010-S.

[28] Srivastava G, Ravi Prakash P. An integrated framework for nonlinear analysis of plane frames exposed to fire using the direct stiffness method. Comput Struct 2017; 190:173–85. https://doi.org/10.1016/j.compstruc.2017.05.013.
[29] EN 1993-1-2. Eurocode 3: Design of steel structures - Part 1-2: General rules - Structural fire design. Brussels: European Committee for Standardization; 2005.
[30] EN 1992-1-2. Eurocode 2: Design of concrete structures - Part 1-2: General rules - Structural fire design. Brussels: European Committee for Standardization; 2004.
[31] Purkiss JA, Li LY. Fire safety engineering design of structures. 3rd Editio. Boca Raton: CRC Press; 2013. https://doi.org/10.1201/b16059.
[32] Ansys. ANSYS Engineering Analysis System. User manual. Canonsburg, Pensilvania: Houston, Pa. : Swanson Analysis Systems, 2019; 2019.
[33] Oñate E. Structural Analysis with the Finite Element Method Linear Statics: Volume 2. Beams, Plates and Shells. 1st ed. Barcelona: Springer; 2013.
[34] Magisano D, Liguori F, Leonetti L, de Gregorio D, Zuccaro G, Garcea G. A quasi-static nonlinear analysis for assessing the fire resistance of reinforced concrete 3D frames exploiting time-dependent yield surfaces. Comput Struct 2019;212:327–42. https://doi.org/10.1016/j.compstruc.2018.11.005.
[35] Kiakojouri F, De Biagi V, Chiaia B, Sheidaii M. Progressive collapse of framed building structures: Current knowledge and future prospects. Eng Struct 2020;206. https://doi.org/10.1016/j.engstruct.2019.110061.
[36] Mattieu J. Asegurar la resistencia al fuego de estructuras metálicas. Segur Contra Incend 2020:1–40.